

CASE FILE COPY

NASA CR-114,495
Available to the public

GROUND EFFECT FOR V/STOL AIRCRAFT CONFIGURATIONS

AND ITS SIMULATION IN THE WIND TUNNEL

PART I INTRODUCTION AND THEORETICAL STUDIES

By J. E. Hackett and E. B. Praytor

Distribution of this report is provided in the interest of information exchange. Responsibility for the contents resides in the author or organization that prepared it.

Prepared under Contract NAS2-6690 by
LOCKHEED-GEORGIA COMPANY
Marietta, Georgia

for Ames Research Center

NATIONAL AERONAUTICS AND SPACE ADMINISTRATION

GROUND EFFECT FOR V/STOL AIRCRAFT CONFIGURATIONS
AND ITS SIMULATION IN THE WIND TUNNEL

Part I Introduction and Theoretical Studies

by J. E. Hackett
and E. B. Praytor

Distribution of this report is provided in the interest of information exchange. Responsibility for the contents resides in the author or organization that prepared it.

Prepared under Contract No. NAS2-6690 by

The Lockheed-Georgia Company,
Marietta, Georgia

for Ames Research Center

NATIONAL AERONAUTICS AND SPACE ADMINISTRATION

TABLE OF CONTENTS FOR PART I

<u>Section</u>	<u>Page</u>
SUMMARY FOR PART I.	1
1. GENERAL INTRODUCTION.	2
2. INTRODUCTION TO PART I.	3
2.1 Scope	
2.2 The potential flow interaction between the ground and a highly-lifting, finite wing.	
2.3 The ground boundary layer	
2.4 Means for tunnel simulation	
3. THE BOUNDARY LAYER ON A MOVING GROUND.	6
3.1 Theoretical prediction method for three dimensional moving ground boundary layers.	
3.2 Correlation with moving ground boundary layer measurements.	
3.3 Effects at the wing.	
4. THE BOUNDARY LAYER ON A FIXED GROUND.	9
4.1 Theoretical predictions.	
4.2 Separation boundaries.	
4.3 Effects at the wing.	
5. THE WALL JET AS AN ALTERNATIVE TO A MOVING GROUND.	11
5.1 Introduction.	
5.2 Early studies of slot size, position and velocity.	
5.3 Reduced slot size and high Reynolds number effects.	
5.4 Effects at the wing.	
6. CONCLUSIONS	15
6.1 Potential Flow	
6.2 Moving ground boundary layers	
6.3 Fixed ground boundary layers	
6.4 The wall jet as an alternative to a moving ground	
REFERENCES	17
FIGURES	19

LIST OF FIGURES FOR PART I

<u>Figure Number</u>		<u>Page No.</u>
1.	Lift Reduction by the Ground Image of a Bound Vortex	19
2.	Floor Pressure Contours for Jet Flap and Externally Blown Flap Configurations	20
3.	Floor Pressure Contours for a C-130 Wing and a Simple Horseshoe Vortex.	21
4.	Velocity Past a Fixed Observer.	22
5.	Ground Boundary Layers as seen by Fixed and Moving Observers.	23
6.	Horseshoe Vortex Geometry for Boundary Layer Studies	24
7.	Boundary Layer Thickness and Wall Shear Stress: Low Reynolds Number, Moving Ground	25
8.	Boundary Layer Thickness and Wall Shear Stress: High Reynolds Number, Moving Ground	26
9.	Moving Ground Boundary Layer Correlation: (i) Boundary Layer Growth	27
10.	Moving Ground Boundary Layer Correlation: (ii) Boundary Layer Velocity Profiles for $V_B/V_\infty = 0.25$	28
11.	Moving Ground Boundary Layer Correlation: (iii) Boundary Layer Velocity Profiles for $V_B/V_\infty = 0.50$	29
12.	Induced Flow, at the Center of the Bound Vortex, Caused by Entrainment into a Moving Ground Boundary Layer.	30
13.	Boundary Layer Thickness and Wall Shear Stress: Low Reynolds Number, Fixed Ground.	31
14.	Boundary Layer Thickness and Wall Shear Stress: High Reynolds Number, Fixed Ground.	32
15.	Separation of a Fixed Ground Boundary Layer for a Uniformly-Loaded, Finite, Unit-Semispan Wing.	33
16.	Induced Flow, At the Center of the Bound Vortex, Caused by Entrainment into a Fixed Ground Boundary Layer.	34

<u>Figure Number</u>		<u>Page No.</u>
17.	Definitions for Wall Jet Velocity Profiles.	35
18.	Base Case for Early Wall Jet Decay Theoretical Studies: $C_{1h}' = 1.58.$	36
19.	Wall Jet Decay On Ground: $C_{1h}' = 2.50.$	37
20.	Wall Jet Decay on Ground: $C_{1h}' = 4.00.$	38
21.	Moving Ground and Wall Jet Velocity Profiles at the Bound Vortex Position: $C_{1h}' = 4.00.$	39
22.	Theoretical Floor Separation Criteria, in Three Dimensions for a Simple, Horseshoe Vortex at Low Reynolds Number.	40
23.	Effect of Slot Height: Low Reynolds Number.	41
24.	Effect of Slot Height: High Reynolds Number.	42
25.	Induced Flow, at the Bound Vortex, Caused by Entrainment into a Wall Jet Used to Simulate a Moving Ground.	43

SYMBOLS FOR PART I

b	wing span
c	wing chord
\bar{c}	wing mean chord
C_F	flap chord
C_f	skin friction coefficient
$C_{f_{MIN}}$	lowest skin friction coefficient found along surface.
C_l	sectional lift coefficient
C_L	wing lift coefficient
C_{l_h}	sectional lift coefficient using reference length h . (See also note below)
$C_{L_{hb}}$	wing lift coefficient using reference area hb .
C_p	static pressure coefficient
C_μ	slot blowing momentum coefficient
h	height, above ground, of wing quarter chord, or bound vortex
K	circulation
L	lift
N	defined in Equation (5.4)
p	local static pressure
p_∞	free-stream static pressure
t	(in Section 2.2): $K/\pi U_\infty h$ (in remainder of report): time
U_∞	free stream velocity
$U(x)$	local, potential flow velocity at the ground.
U_G	velocity of surface of moving ground
U_m	wall jet maximum velocity. See also Figure 17.

u	horizontal perturbation velocity
	vertical perturbation velocity
x	distance from origin of boundary layer, or from blowing slot exit
x _{SEP}	horizontal distance between fixed ground separation point and bound vortex. See also Figure 15.
x _{SLOT}	horizontal distance between the blowing slot exit and the bound vortex
x _p , y _p	coordinates of the bound vortex
α	wing incidence
δ	boundary layer total thickness. Taken as 0.995 U(x) and 1.005 U(x) for fixed and powered boundary layers respectively.
δ*	boundary layer or wall jet displacement thickness.
δ _F	flap deflection angle
ρ	air density

Note: C_{l_h}' is a sectional lift coefficient which excludes the effects of ground-image-vortex-induced counterflow. The prime, in effect, converts C_{l_h} to a circulation coefficient, equal to $2K/U_{\infty}h$. The relationship between the two quantities, which, may be derived from Equation (2.1), is:

$$C_{l_h} = C_{l_h}' - (C_{l_h}'^2 / 8\pi)$$

$C_{l_{hb}}'$ is the corresponding circulation coefficient for three-dimensional cases. It is not related to $C_{l_{hb}}$ in a simple manner.

The definitions of C_l , C_{l_h} , C_{l_h}' , $C_{l_{hb}}$, and $C_{l_{hb}}'$, in Parts II and III of this report, are the same as those above.

GROUND EFFECT FOR V/STOL AIRCRAFT CONFIGURATIONS AND ITS
SIMULATION IN THE WIND TUNNEL

Part I Introduction and Theoretical Studies

By J. E. Hackett and E. B. Praytor

SUMMARY

Theoretical studies are made of three dimensional turbulent boundary layer behavior on fixed grounds and on moving grounds of the type used in wind tunnel tests. It is shown that, for several widely-varying STOL configurations, the ground static pressure distributions possess a remarkable degree of fore-aft symmetry about the center of lift. At low Reynolds number, corresponding to small-tunnel testing, the boundary layer displacement surface reflects to a large degree the symmetry of the pressure distribution. For this reason, induced incidence at the model is small for unseparated ground flow. At high Reynolds number, the displacement thickness decrease aft of the static pressure maximum is noticeably more rapid than the corresponding rise. This is attributed to trailing-vortex-induced "spanwise pumping" within the boundary layer.

Entrainment into the moving ground boundary layer is small, even at high lift levels. This eases the task of simulating the moving ground by other means. Because ground static pressures up to stagnation can be present, the use of suction boundary layer control is not recommended. Blowing boundary layer control studies centered around the hypothesis that the wall jet maximum velocity, at the maximum static pressure position, should equal the mainstream velocity at infinity. It was found possible to generate a family of closely similar wall jet decay curves, over the model lift range of interest, by specifying the initial wall jet super-velocity as a multiple of the maximum bound-vortex-induced countervelocity at the ground surface.

Experimental verification is required for the single-slot, wall-jet-blowing hypothesis and the supervelocity rule tentatively suggested here. Part II will be devoted to this.

1. GENERAL INTRODUCTION

The importance of ground effect to V/STOL vehicle performance has long been recognized. Though moving ground belts have been used in some wind tunnels for many years, significant "grey areas" remain concerning when they are necessary and what the consequences are of transgressing known boundaries. There is a tendency to avoid the difficulties, costs and inconveniences of belt-type moving ground operation and substitute fixed ground tests, with the sometimes-slender hope that the consequences will not be serious.

Where a moving ground is not used routinely, there are three essential steps toward obtaining valid ground effect measurements. These concern firstly recognition that floor separation may occur (or has occurred), then judgement whether serious errors will result and, finally, solution of the flow problem by using a moving belt or other means. Several authors have examined the problem and suggested criteria for predicting when fixed-ground testing becomes unreliable. (See References 1 to 5). However, the consequences of pressing fixed ground testing too far are less well demonstrated (but see Reference 5) and the authors are aware of no available studies concerning the use of alternative means to the conventional, moving-belt type of simulation.

It is the major aim of this total study to examine means of providing proper simulation of a moving ground without actually using one. To this end, theoretical, experimental and design studies have been made which are documented in parts I, II and III respectively of this report. Part III will include design notes and suggested operating procedures for a floor boundary layer control system designed for use in the NASA Ames 40' x 80' wind tunnel.

2. INTRODUCTION TO PART I

2.1 Scope

A theoretical study of moving and fixed ground boundary layers is a desirable prerequisite in the search for a viable, boundary-layer-controlled system which takes the place of the moving belt type of simulation. Since the correct condition for ground effect testing is with a moving ground, this is regarded as the norm and its study will be discussed first, in Section 3. Sections 4 and 5 will be devoted to fixed ground boundary layers and wall-jet development respectively. Section 6 will draw conclusions from the theoretical studies.

The choice of configurations for study is necessarily highly selective. Fortunately the configuration of primary interest - the finite, high-lift wing - is amenable to analysis. The philosophy adopted will be to develop a sufficient understanding of the most severe wing cases to permit the design of meaningful experiments on an alternative system to a moving ground. Extrapolation to a lifting jet case (for example) will then be accomplished by experiment.

2.2 The potential flow interaction between the ground and a highly-lifting, finite wing.

Before any consideration of boundary layers, it is appropriate to review the potential flow pressure fields concerned. Consider the center section of a straight, high aspect ratio wing at an altitude of about one chord length. Though this section "sees" the whole of the ground image system, the predominant effect is due to the bound vortex image. Regarding the wing as a point vortex and arbitrarily increasing its strength, increasing static pressure is experienced at the ground. Eventually this flow stagnates and a (potential flow) separated cavity occurs (see Figure 1). At the same time, counterflow at the wing, induced by the image bound vortex, reduces the horizontal velocity there and wing lift falls below the free air value. The decrement is given by the second term in the equation:

$$C_l = 2\pi \frac{h}{c} \left(t - \frac{1}{4} t^2 \left(1 + 16 \left(\frac{h}{b} \right)^2 \right)^{-1/2} \right) \quad (2.1)$$

where b , c , and h are the wing span, chord and altitude respectively and the circulation parameter, t , is defined by:

$$t = K / \pi U_\infty h \quad (2.2)$$

At the wing tip, the image-induced counterflow at the bound vortex is almost halved and it may be shown that, once again for given circulation, K ;

$$C_l = 2\pi \frac{h}{c} \left(t - \frac{1}{8} t^2 \left(1 + 4 \left(\frac{h}{b} \right)^2 \right)^{-1/2} \right) \quad (2.3)$$

Equations (2.1) and (2.3) are plotted in Figure 1 for the limit of large aspect ratio. Two major points may be made. Firstly, root and tip lift coefficients C_{lh} are limited to maxima of 2π and 4π respectively. Beyond these points, further increases in circulation (assuming this to be possible) reduce lift. Sectionally, the wings of several contemporary STOL designs operate in the regime marked "A" in Figure 1. This raises the second major point: there may be occasions when "separation" of the potential flow is correct, even with a moving ground. However the detailed results here should be regarded as qualitative because of the simplifying assumptions.

So far, it has been assumed that circulation may be generated at will and with equal ease at root and tip. In practice, the available bound circulation is likely to be proportional to the horizontal velocity over the wing. This increases the tendency for the root to lose lift faster than the tip as the ground is approached.

Trailing vortex effects, not so far considered, are responsible for the more familiar positive lift interference, caused by ground-induced upwash, which predominates for more modest lift coefficients and greater altitudes. In contrast to bound image effects, trailing vortex images tend to centralize lift.

Figures 2 and 3 show calculated floor pressure contours for a variety of wing configurations. These were calculated using vortex lattice techniques which included the use of an "equivalent flap" concept for the powered cases. Lift coefficients are generally modest (by STOL standards) in these figures, because means are not yet available for analyzing cases involving floor impingement of the jet sheet. Even so, the maximum static pressure coefficients concerned would separate a fixed-ground boundary layer. The lower part of Figure 3 shows the pressure "footprint" of a simple horseshoe vortex placed at a representative altitude. The pressure distribution is almost two-dimensional over much of the span and possesses strong fore-aft symmetry about the bound vortex position.

2.3 The Ground Boundary Layer

It is not always clearly understood that there is a boundary layer on a moving ground situated beneath a lifting model. From the viewpoint of an observer standing on the ground, who sees an aircraft passing overhead, there is flow in the flight direction which is greatest when the aircraft is directly above. Figure 4 shows likely velocity-time histories at various heights. Because of this motion of air over the fixed ground, viscous effects come into play and a time-varying boundary layer is seen by the fixed observer. However, if an axis system is chosen which moves with the aircraft, the problem is transformed into a steady one (see Figure 5). Within this frame of reference, the curves of Figure 4 still represent the velocity difference between the moving ground and the potential flow above it, but now as a function of distance.

The static pressure maximum, under the bound vortex, coincides with the peak velocity difference between the moving ground and the potential flow. Thus, the ability of the moving ground to supply energy to the flow is greatest at the

position where a fixed ground boundary layer is most prone to separate. The moving ground is able, inherently, to provide boundary layer control which is appropriate to the particular pressure distribution which is imposed upon it. However, it has not been clear whether, while doing this, the moving ground is "seen" by the model as an active device which modifies the potential flow via entrainment, or whether it has a more passive effect. This will be investigated in Section 3.

2.4 Means For Tunnel Simulation

Unquestionably, the best known way to simulate a moving ground is to use the familiar, full-span conveyor-belt type of device. Where this is not possible for operational or other reasons it is likely that alternative mechanical devices might be precluded for similar reasons. One possible alternative - which has no rotating parts - would be a compliant ground, arranged to reduce adverse pressure gradients and thereby prevent fixed ground separation. However this fails by definition since it removes those same high ground pressures which cause the interference which is of interest.

Boundary layer control may also be considered. This must prevent separation and also (possibly) emulate the entrainment action of the equivalent moving ground boundary layer. Passive BLC devices are clearly not sufficient in pressure fields like those of Figures 2 and 3, which leaves the inevitable choice between suction and blowing BLC. Distributed suction has considerable appeal since "tailoring" is possible in relation to the pressure distribution and power requirements are generally smaller. However, there is virtually no relevant boundary layer control experience and no available prediction method involving such high static pressure gradients as those found in Figures 2 and 3.

Distributed tangential blowing, on the other hand, has obvious physical appeal. In principle, slots could be arranged so that a layer of air next to the ground has always maintained at the same speed as a moving belt. Energy addition of this sort has a much better potential for preventing boundary layer separation. There would also be at least a chance of simulating conditions (mentioned in subsection 2.2) where a "potential flow" type of separation should occur.

There are three questions which are approachable theoretically:

(i) Is a moving ground essentially active or passive? This was posed earlier and will be dealt with below.

(ii) Under what conditions is moving ground simulation needed? A fixed ground study in Section 4 will provide guidance on this.

(iii) Can slot blowing boundary layer control adequately simulate moving ground conditions? A study in Section 5 will be made paying particular attention to the importance of simplicity in any practical scheme.

3. THE BOUNDARY LAYER ON A MOVING GROUND

3.1 Theoretical Prediction Method for Three Dimensional Turbulent Moving Ground Boundary Layers.

In Reference 4, a fixed-ground three dimensional turbulent boundary layer calculation scheme by J. F. Nash was used successfully to predict boundary layer development on the ground beneath a 13-foot span C-130 wind tunnel model. A book on the boundary layer fluid mechanics and calculation methods used has recently been published by Nash and Patel (Ref. 7). The program used in Reference 4 has been modified, for the present work, by replacing the fixed ground boundary condition by a surface moving at a prescribed speed.* It is thus possible to calculate off-speed results, including the zero speed fixed ground as a special case.

A thick, conventional initial turbulent boundary layer was assumed in early developmental runs. The much smaller scale moving ground boundary layer developed beneath this. It was found that the upper part of the original profile remained recognizable for all of the streamwise distance of interest. More importantly, there were serious theoretical doubts related to the fact that two quite distinct length scales were always present: strictly, provisions should be made to handle the these separately. Such a calculation is beyond the current state-of-the-art. Thin, "relaxed" moving ground profiles were therefore used routinely for initialization. This corresponds to wind tunnel boundary layer removal just upstream of the beginning of the moving ground.

In the same way as described in Reference 4, a vortex lattice representation of a wind tunnel model may be input to the program. The program calculates the ground pressure distribution, for the altitude specified, then proceeds with a three dimensional boundary layer calculation. Several types of output are possible including boundary layer velocity and shear stress profiles, mean boundary layer parameters, displacement surface details and induced flows at the model due to the displacement surface. Some limited correlations made with experimental data will be discussed in Subsection 3.2.

Theoretical studies were made at two Reynolds numbers, corresponding to the small scale experiments to be described in Part II and to the test conditions in the NASA Ames 40' x 80' wind tunnel. The geometry used for these studies is both greatly simplified and conservative. (See Figure 6). The lack of sweep, the uniform span loading and the close proximity to the ground (intended to be about one mean chord for an aspect ratio six wing) all combine to produce a particularly severe case so far as the boundary layer is concerned.

Figure 7 shows a set of low Reynolds number results. The total thicknesses, δ , become appreciable as C_{lh} is increased. However, since δ is the one-half-percent-deviation thickness, there is little chance of significant mean effects at the model for the cases in Figure 7.

The displacement thickness of a moving ground boundary layer is, of course, negative: what the model "sees" in hard surface terms is a hollow in the floor

* See Appendix.

which represents the entrainment action of the boundary layer. At a C_{lb}^i of five, the depth of this hollow has reached 16% of model height. The consequences at the model will be discussed in Subsection 3.3.

A rather remarkable property of the displacement thickness and skin friction curves in Figure 7 is their degree of fore-aft symmetry. Though the symmetry of the static pressure distribution has already been mentioned (see Figure 3(ii)), the almost-elastic response of the boundary layer displacement thickness might not have been expected. The implication for exactly symmetric profiles is that they will induce camber and horizontal velocity effects at the model but no incidence increment.

Figure 8 repeats the conditions of Figure 7, except that Reynolds number is much higher. Here, the thicknesses are somewhat smaller, as would be expected, but the fore-aft boundary-layer symmetry has also changed. Examination of off-center velocity profiles shows that, in these cases, significant cross-flow super-velocity develops in the boundary layer downstream of the bound vortex. This "bleeds" the central boundary layer, reducing the physical and displacement thicknesses more markedly than at low Reynolds number. The impact on induced flows at the model will be discussed in Subsection 3.3.

3.2 Correlation With Moving Ground Boundary Layer Measurements

Ideally, correlations should be made against tests on finite-span, high lift models of several feet span at high Reynolds number. Large scale tests were attempted, on a "piggy back" basis during tests on an externally-blown flap model in the Lockheed-Georgia Low Speed Wind Tunnel. Some pilot data were obtained, but operational problems prevented further work. No small scale tests were attempted.

Roper and Gentry (Reference 8) give data from large scale moving belt tests, in zero pressure gradient, carried out at NASA Langley. Tunnel speed was 100 ft/sec approximately and boundary layer profiles were measured at various stations for a range of underspeed belt conditions. The belt material was stated to be aerodynamically rough, but no numerical value was stated. Roughness was therefore established, for the present study, via a matching process involving fixed ground experimental/theoretical comparisons.

The results of an initial correlation attempt, which assumed complete removal of the initial boundary layer, were disappointing. However the use of the 4.5 foot experimental velocity profile to start the theoretical calculation gave more satisfactory results, even though the shear stress profile had to be estimated. Because of this an initial transient is evident in Figure 9 which settles out as the shear stress and velocity profiles find equilibrium. Once this has occurred, there is reasonable agreement between predicted and experimental boundary layer thicknesses. The corresponding velocity profiles are given in Figures 10 and 11 and show adequate agreement for the present purposes.

3.3 Effects At The Wing

If the slope of the boundary layer displacement surface is $d\delta^*/dx$ and the model coordinates are (x_p, y_p) , the velocity components, u, v induced at the model are given by

$$\frac{u}{U_\infty} = \frac{1}{\pi} \int_{-\infty}^{\infty} \frac{U(x)}{U_\infty} \left(\frac{d\delta^*}{dx} \right) \frac{(x_p - x) dx}{(x_p - x)^2 + y_p^2} \quad (3.1)$$

and

$$\frac{v}{U_\infty} = \frac{1}{\pi} \int_{-\infty}^{\infty} \frac{U(x)}{U_\infty} \left(\frac{d\delta^*}{dx} \right) \frac{y_p dx}{(x_p - x)^2 + y_p^2} \quad (3.2)$$

where $U(x)$ is the local velocity just outside the boundary layer.

The equations are for two-dimensional flow. However, the displacement surfaces corresponding to Figures 7 and 8 are sufficiently two dimensional for the use of Equations (3.1) and (3.2) to produce little error. For more three-dimensional cases, there will be an overestimate in u and v .

Algorithms were added to the moving ground program which evaluated the above integrals numerically. For early calculations the $U(x)/U_\infty$ term was left out. However this caused significant overestimates in u and v and the full equations have been employed since. No attempt has been made to feed back the displacement effects into the potential flow.

Figure 12 shows vertical and horizontal induced velocities, at the center of the bound vortex, as functions of lift coefficient C_{lh}' . As suggested above, the boundary-layer-induced vertical relative velocity at the model was very small at low Reynolds number - of order 10^{-4} . This contrasts with the high Reynolds number case where the value approaches $\frac{1}{2}\%$ of freestream velocity. The induced angle will be more greatly affected, because of counterflow effects.

Horizontal induced velocities at the model, in contrast, are very similar at high and low Reynolds numbers. At low Reynolds number the boundary-layer-induced counterflow at the model slightly exceeds 3% at a C_{lh}' of five.

It is evident that until quite extreme conditions are reached, the induced flows at the model position, caused by boundary layer entrainment at the moving ground, are small. The predominant role of the moving ground is thus to prevent separation. This fact makes much easier the task of finding an alternative, but equivalent, boundary layer control system.

4. THE BOUNDARY LAYER ON A FIXED GROUND

4.1 Theoretical Predictions

Fixed ground boundary layers are of interest here mainly because their behavior defines when a moving ground or its equivalent is needed. It is of additional interest to examine trends in C_{lh}' and C_p values for separation as model height and Reynolds number are varied. The greater detail accessible in good theoretical analyses is helpful in understanding the mechanisms, both pre- and post-separation, which affect the flow at the model.

The fixed ground three dimensional turbulent boundary layer program **used** took two forms. The first was essentially that employed in Reference 4, the second was the previously-mentioned moving ground program applied at zero belt-speed. There was close agreement between results derived using the two programs for fixed ground cases.

Figure 13 is the fixed-ground equivalent of Figure 7. Skin friction and displacement thickness are of course positive for the fixed ground, but the comments regarding fore-aft symmetry are the same. Ground separation provides a limit to C_{lh}' beyond which calculations cannot be made.

Comparisons between Figures 8 and 14 once again show high Reynolds number steepening of the aft displacement surface.

4.2 Separation Boundaries

In the present work "separation" has been assumed to occur when the streamwise component of wall shear stress vanishes. In more highly three-dimensional flows this assumption might be questionable; however no ambiguity should exist in boundary layers of the type considered here.

The upper part of Figure 15 illustrates the determination of separation C_{lh}' via extrapolation of the minimum value of skin friction to zero. A second method is also illustrated which extrapolates back from already-separated, higher C_{lh}' conditions to determine where the separation distance, x_{SEP} , becomes zero. Though invalid beyond separation, errors decrease at lower x_{SEP} values and extrapolation to zero appears to yield acceptable results. Similar studies produced the following results:

Model Height \ Approach Re.	1.019 Million	28.8 Million	} C_{lh}' at ground separation
0.168	1.83	2.32	
0.337 ("Double Height")	2.42		

C_{lh}' is clearly by no means a universal function for the definition of separation. The values above are significantly below those suggested in References

1 and 2, for example, though the near-ground, uniform span load condition is admittedly untypically severe. Nevertheless the variations with height and Reynolds number must be considered significant. A further study, illustrated in Figure 22, will be discussed in Section 5.3.

4.3 Effects At The Wing

Figure 16, which corresponds to Figure 12 for the moving ground, shows velocity increments induced at the model by the fixed ground boundary layer displacement surface.

It has already been mentioned that separation prevents full boundary layer calculations once it occurs. For interest, however, post-separation values of u and v were calculated for the portion of the boundary layer ahead of the separation point. The result illustrates an earlier point, that the lack of cancellation effects from the aft boundary layer leads to significant additional induced incidence beyond that due to the separation streamline itself. Prior to separation, the induced vertical velocity increments are small and less Reynolds number sensitive than with the moving ground.

Horizontal velocity increments, on the other hand, are of quite significant size even at quite modest (pre-separation) C_{lh} values. Nevertheless it is the occurrence of separation which provides the most serious deficiency of the fixed ground.

5. THE WALL JET AS AN ALTERNATIVE TO A MOVING GROUND

5.1 Introduction

At the end of Section 2, three questions were posed. The first was answered in Section 3, where it was shown that the action of a moving ground is essentially passive, rather than active (So far as the model is concerned, that is). The second question, relating to conditions under which moving ground simulation is required, was partly answered in the previous section. This will be extended experimentally in Part II of this report.

What remains in this theoretical study is to investigate the feasibility of and suggest design details and operating procedures for simulating a moving ground by means of a single wall jet or multiple wall jets. For obvious reasons, the former is highly desirable, so this will be investigated initially.

Reference 9 is a theoretical wall jet study which includes comparisons with experiment for adverse pressure gradient conditions. The computer program given there was implemented and modified for vortex-induced pressure distributions and improved input/output. The program is for two dimensional flow, so the results will not be directly comparable with those previously described, but nevertheless will be conservative. No comparable three dimensional program was available.

The central theme of the studies described in Section 5 concerns the hypotheses that:

(i) It is conditions directly under the bound vortex which are the most significant. (This is the first place to separate.)

(ii) The peak wall jet velocity U_m (See Figure 17), under the bound vortex, must equal mainstream speed. This is suggested by the fact that the supply of energy from a moving ground to the mainstream is strongly related to the local velocity difference between the two. The peak wall jet velocity under the bound vortex must therefore at least approximately equal that of the moving ground it replaces.

In the following subsections, means of achieving (ii) are determined. The hypotheses obviously must then be put to experimental trial.

5.2 Early Studies of Slot Size, Position and Velocity

Initial studies were focussed on determining slot size and velocity, for cases comparable with those discussed previously, which are experimentally reasonable at small scale and also economical in power. A major aim was to determine suitable operating rules for varying the three slot parameters as $C_{L_{hb}}$ is varied. The criterion for good operating rules is that the non-dimensional behavior of the wall jet maximum velocity, relative to the equivalent moving ground condition, should be the same or closely similar over the entire C_{lh} range of interest.

(i) Distance to blowing slot, x_{SLOT}

In order to avoid fixed-ground separation, it is clear that the injection position should be a function of bound vortex circulation. The point where C_p is approximately 0.15, which is conservative, was chosen in initial studies. A good approximation to this is given by

$$\frac{x_{\text{SLOT}}}{h} = 3.54 C_{p_{\text{MAX}}} \quad (5.1)$$

where

$$C_{p_{\text{MAX}}} = 1 - \left(1 - \frac{c_{1h}'}{2\pi}\right)^2 \quad (5.2)$$

(ii) Slot height.

This, too, could be scaled as above. However, studies showed this did not produce the desired type of wall jet behavior and constant values were used subsequently. This constancy has obvious mechanical and supply-matching advantages.

(iii) Blowing velocity.

The difference between the moving ground velocity and the potential flow velocity directly beneath the vortex is given by

$$\left(\frac{U_G - U}{U_\infty}\right)_{\text{MAX}} = \frac{2K}{2\pi U_\infty h} = \frac{c_{1h}'}{2\pi} \quad (5.3)$$

where U_G is the moving belt speed and U is the potential flow velocity, at the ground, directly below the bound vortex.

The aim is to arrange the slot blowing velocity in such a way that

$$\left(\frac{U_m - U}{U_\infty}\right)_{\text{MAX}} = \frac{c_{1h}'}{2\pi} \text{ under the bound vortex.}$$

To allow for decay, the superevelocity at the blowing slot must be several times this value. Therefore we specify that, at the slot,

$$\left(\frac{U_m - U}{U_\infty}\right)_{\text{SLOT}} = N \frac{c_{1h}'}{2\pi} \quad (5.4)$$

where N will be a function of slot height. This yields

$$U_{m\text{SLOT}} = U_{\infty} \left(1 + N \frac{C_{1h}'}{2\pi} \right) \quad (5.5)$$

on assuming that U_{slot} , the local mainstream velocity just above the slot is closely equal to U_{∞} .

Exploratory runs with the wall jet program lead to a suitable slot height and velocity combination for the base case shown in Figure 18. In the upper part of the figure, $(U_G - U)$ can be regarded as a "target" velocity distribution along the ground: it is this difference which "drives" a moving boundary layer. The decay curve $(U_m - U)$ may be regarded as properly matched when it passes through the peak in the $(U_G - U)$ curve: U_m , under the model, then equals U_{∞} . The blowing velocity in Figure 18 corresponds to an N value of 3 in Equation (5.4) above. This can probably be reduced, in the interests of power economy, so that the decay curve intersects the crest of the $(U_G - U)$ curve.

The C_{1h}' value in Figure 18 is modest and in a real test a fixed ground might be adequate. Increasing C_{1h}' to 2.5 and 4.0 in Figures 19 and 20 respectively shows that Equation 5.4 may be used with confidence to relate slot blowing velocity to model lift.

The maximum C_p value of 0.87 in Figure 20 is also worth comment: it is highly unlikely that suction boundary control could be applied successfully in this situation.

Finally, we note that the maximum displacement thickness of the wall jet has become significant. Reference to Figure 21, which shows comparable moving ground and wall jet velocity profiles, shows that the latter has a substantially fuller profile. The corresponding velocities induced at the model will be examined in Subsection 5.4.

5.3 Reduced Slot Size and High Reynolds Number Effects

Design studies for the NASA Ames 40' x 80' wind tunnel, described in Part III of this report, laid emphasis on high Reynolds number, lower relative slot height (for pressure/mass flow matching to the supply) and blowing from as close to the model as possible (for power economy).

Figure 22 extends the study of Section 4 and shows that, even at low Reynolds number, the slot position may safely be moved aft to the 0.3 contour. The relation between $Cl_{hb\text{SEP}}'$ and h/b is also particularly interesting. This dependence is related primarily to the rounding of the floor pressure contours and reduction in the pressure peak as model height is increased.

Additional, two dimensional, wall jet runs were made changing one parameter at a time so that the separate effects of the several changes mentioned could be

determined. The value of $C_{p\text{slot}}$ was increased by increasing model height while maintaining both slot position and C_{lh} constant. This technique was used for experimental hardware reasons and to improve the shape of the $(U_m - U)$ velocity decay curve.

Figure 23(b) is for a slot with the same thrust (i.e. $C_{U\text{SLOT}}$) as Figure 23(a) but with only 40% of the slot height. The decay curve is slightly higher in some places but there is little overall difference. This conclusion was later checked experimentally.

Figure 24(a) repeats the comparison shown in Figure 23, but at high Reynolds number. Length and speed scales, multiplied by 12 and 1.52 respectively, correspond to typical 40' x 80' tunnel length scale and 90 kts. Once again, differences due to decreased slot size at constant C_{lh} are not large, though they are somewhat more noticeable than at the lower Reynolds number. The most significant feature in Figure 24(a) is the high Reynolds number benefit to the value of N required for matching. The reduction from 3 to about 2.5 implies a 30% slot power reduction, at this $C_{I_{hb}}$ value, or a 10 kt forward speed increase at constant power.

Though N values of 2 and 3 have been retained above for the sake of continuity it is incorrect to apply these in Equation 5.5 for the smaller slot cases. The values given below Figures 23(b) and 24(b) are the appropriate ones.

5.4 Effects at the Wing

Algorithms for induced velocity at the wing were added as before. A conservative, small-slot high-blowing case ($N = 3$) was used as a base (see Figures 23 and 24). The addition of further C_{lh} cases permitted comparison with the corresponding moving ground cases.

Once again the induced vertical velocities are an order of magnitude smaller than the horizontal velocities (see Figure 25). The induced horizontal velocities are remarkably similar to the moving ground values (Figure 12), despite the widely-differing velocity profiles. Bearing in mind that a conservative wall jet case was chosen, we conclude that little difference should be noticed in overall effects at the model whether a moving ground or a properly-matched wall jet is employed. As far as is possible without experiment, this confirms the hypothesis made in Sub-section 5.1.

6. CONCLUSIONS

6.1 Potential Flow

1. As wing bound circulation is increased in ground effect, countervelocities at the ground can exceed the mainstream velocity. Even with a moving ground, a "separation" bubble is then possible.
2. Under these conditions it is unlikely that successful boundary layer control can be achieved via suction as an alternative to a moving ground.
3. There is significant fore-aft symmetry in ground static pressure contours for several wing configurations. (See Figures 2 and 3).

6.2 Moving Ground Boundary Layers

4. The velocity difference between a moving ground and the potential flow above it is inherently such that most energy is supplied to the fluid at places where adverse conditions are greatest for the boundary layer. The moving ground thus has the nature of a carefully-applied boundary layer control system.
5. The three dimensional turbulent boundary layer program by J. F. Nash (see References 4 and 7) has been applied successfully to the moving ground boundary layer. Checks against available data in NASA TMX2515 (Ref. 8) have lent confidence to its use in the present investigation.
6. Studies using the Nash program show that, so far as the wing is concerned, the moving ground acts in an essentially passive, but separation-suppressive manner. Simulation via boundary layer control is therefore not precluded.
7. There is significant fore-aft symmetry in the boundary layer displacement surfaces both with moving and fixed grounds. This reflection of the fore-aft symmetry of the pressure distribution is less marked at high than at low Reynolds numbers.
8. As a result of displacement surface fore-aft symmetry, horizontal induced velocity increments at the model position tend to be an order of magnitude greater than the vertical increments.

6.3 Fixed Ground Boundary Layers

9. The parameter Cl_{hb} , sometimes quoted as a criterion for tunnel flow breakdown, is not sufficiently descriptive for close-to-ground conditions. Here, typically lower values have been found than suggested in Reference 2, which are functions of both model height to span ratio and Reynolds number (see Section 4.2 and Figure 22).

10. It is the occurrence of flow separation, as opposed to boundary layer thickening, which limits the high lift capability of the fixed ground board. This is because, in addition to separation-streamline-induced effects at the model, there is a forward-boundary-layer-induced increment which is no longer nullified by a corresponding opposite contribution from the aft boundary layer.

6.4 The Wall Jet As An Alternative to a Moving Ground.

11. A hypothesis has been made that, for successful simulation of a moving ground using a wall jet, the peak wall jet velocity under the bound vortex must equal the free stream velocity at infinity. The hypothesis has been confirmed by theoretical studies; experimental checks will be described in Part II of this report.
12. To achieve the above conditions, a parametric study showed that a slot is required placed on the $C_p = 0.3$ static pressure contour and with a blowing velocity given by Equation (5.5). An almost-similar family of wall jet decay curves is then obtained over the required lift range.
13. Despite the very much fuller wall jet velocity profiles and larger (negative) displacement thicknesses, the induced velocities at the model position were sufficiently small to permit the experimental investigation of Part II to be approached with confidence.
14. Though the wall jet boundary layer predictions showed total thicknesses occupying a significant proportion of model height, only at quite high C_{lh} values (≥ 5) did it appear that direct interference with the wing is likely to cause difficulty.
15. The overall conclusion to the theoretical study is that the use of a wall jet to simulate a moving ground is theoretically feasible, using procedures described in Section 5. The round jet and impingement cases generally must be investigated experimentally. The hypothesis mentioned in Conclusion 11, above, must also be subjected to experimental test.

7. REFERENCES

1. Heyson, Harry H.: Theoretical Study of Conditions Limiting V/STOL Testing in Wind Tunnels With Solid Floor. NASA TN D-5819 June 1970.
2. South, P.: Measurements of Flow Breakdown in Rectangular Wind Tunnel Working Sections. Aeronaut. Rep. LR513 (NRC No. 10616), Nat. Res. Council. Can. (Ottawa), Nov. 1968.
3. Tyler, R.A. and Williamson, R.G.: Tunnel Flow Breakdown from Inclined Jets. Aeronaut. Rep. LR545, Nat. Res. Council. Can. (Ottawa), March 1971.
4. Hackett, J.E.; and Justice, J.L.: The Aerodynamics of a Fixed Ground Plane for a Powered STOL Wind Tunnel Model, AIAA Paper 71-266. March 1971.
5. Turner, T.R.: A Moving Belt Ground Plane for Wind Tunnel Ground Simulation and Results for Two Jet Flap Configurations. NASA TN D4228, 1967.
6. Lazzeroni, F.A.; and Carr, L.W.: Problems Associated With Wind Tunnel Tests of High Disk Loading Systems at Low Forward Speeds. Aerodynamics of Rotary and V/STOL Aircraft. Vol II - Wind Tunnel Testing New Concepts in Rotor Control, Cornell Aeronaut. Lab., Inc., and U.S. Army Aviat. Mat. Lab., June 1969.
7. Nash, J.F.; and Patel, V.C.: Three Dimensional Turbulent Boundary Layers. Published by SBC Technical Books, Inc. Atlanta. 1972.
8. Roper, A.T.; and Gentry, C.L.: Turbulent Boundary Layer Development on a Moving Belt of Rough Texture. NASA TM X-2515 April 1972.
9. Harris, G.L.: The Turbulent Wall Jet in a Moving Stream. NATO AGARD ograph No. 97, page 131, May 1965.

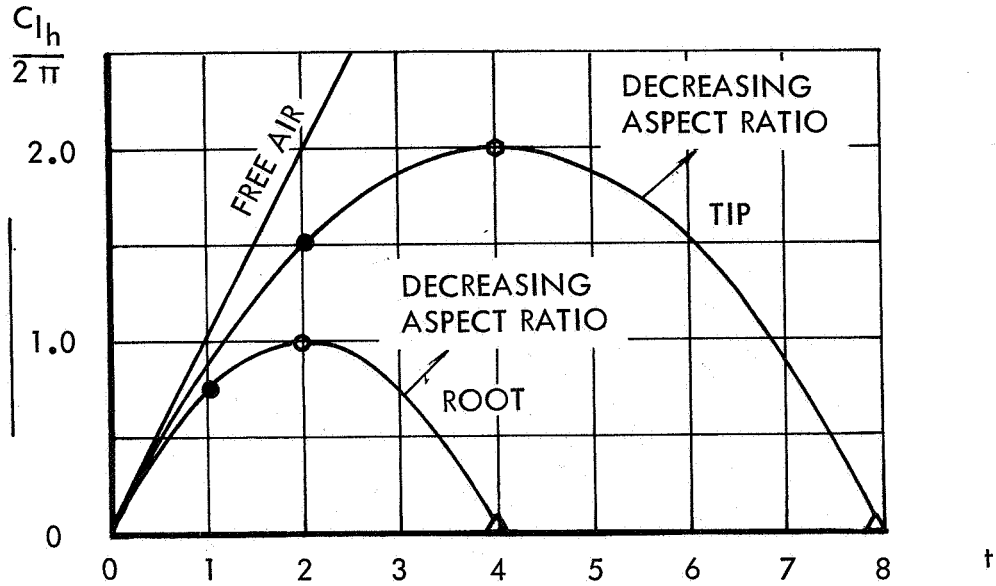
APPENDIX (J. F. Nash)

Boundary-Layer Calculation Method

The calculation method for three-dimensional turbulent boundary layers is based on the numerical integration of the time-averaged equations of motion: the two mean-flow momentum equations, and the continuity equation. The Reynolds stresses are determined from a parallel numerical integration of a pair of empirical rate equations which model the production, transport, and dissipation of the kinetic energy of the turbulence.

The five governing equations are integrated in a three-dimensional domain to yield the solution which consists of the spacial distribution of the three, orthogonal mean-velocity components and the two turbulent shear-stress components. Three-dimensional velocity profiles are produced at specified positions on the surface, and values of wall shear-stress (magnitude and direction), boundary-layer thickness, and displacement thickness are generated at closely spaced stations.

Further details of the method, as applied to fixed walls, are given in Reference 7. The extension to moving walls, for the purposes of the present work, consisted of a change of wall boundary condition, and the redefinition of boundary-layer thickness and diffusion function in terms of the difference between wall velocity and the velocity at the outer edge of the boundary layer. Otherwise the method, the explicit numerical scheme, and the empirical turbulence functions were identical to those described in Reference 7.



NOTE: $C_{l_h} = \frac{L}{\rho U_\infty^2 h}$ $t = \frac{k}{\pi U_\infty h}$

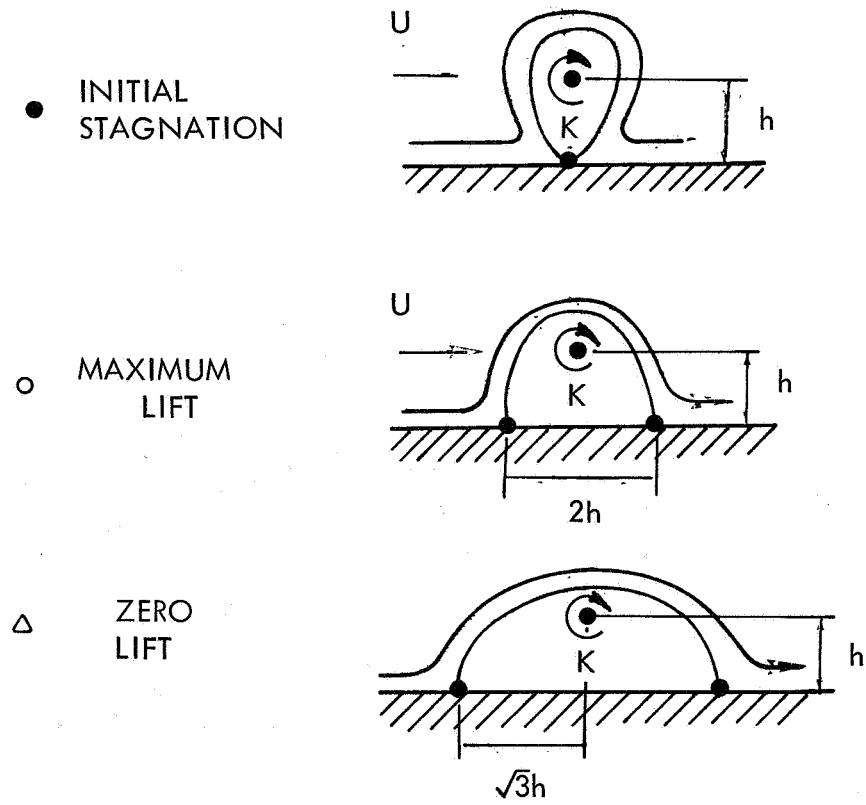
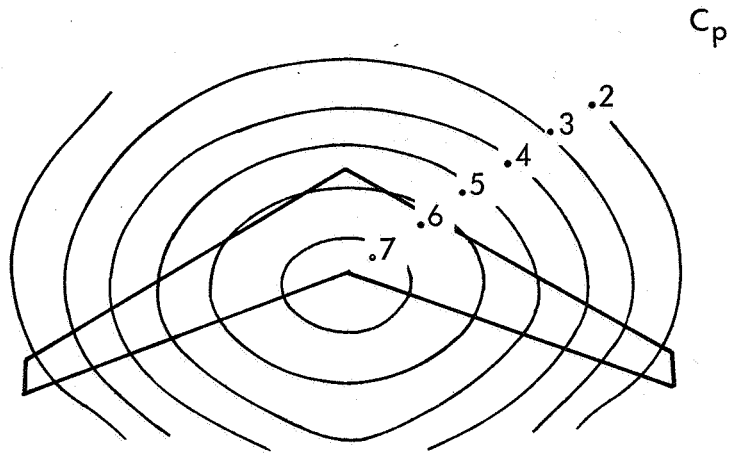
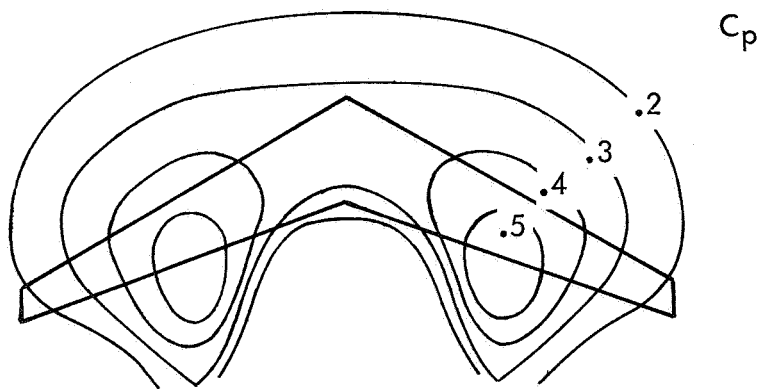


FIGURE 1 LIFT REDUCTION BY THE GROUND IMAGE
OF A BOUND VORTEX



(a) Jet Flapped Wing at $\frac{h}{c} = 2.0$ $C_L = 4.93$

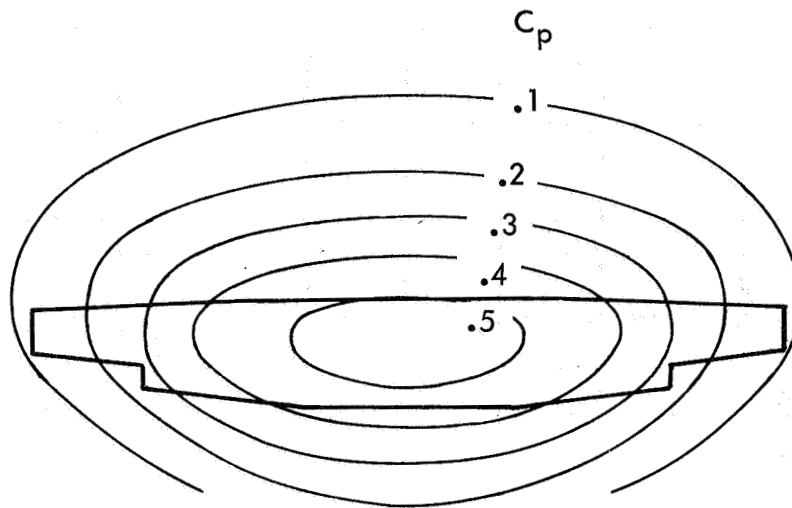
$\alpha = 15^\circ$ $\delta f = 60^\circ$ Full span blowing at $C_{\mu} = 1.0$



(b) Externally Blown Flap Configuration at $\frac{h}{c} = 2.0$ $C_L = 3.21$

$\alpha = 0^\circ$ $\delta f = 60^\circ$ Central 50% of semispan $C_{\mu} = 2.0$

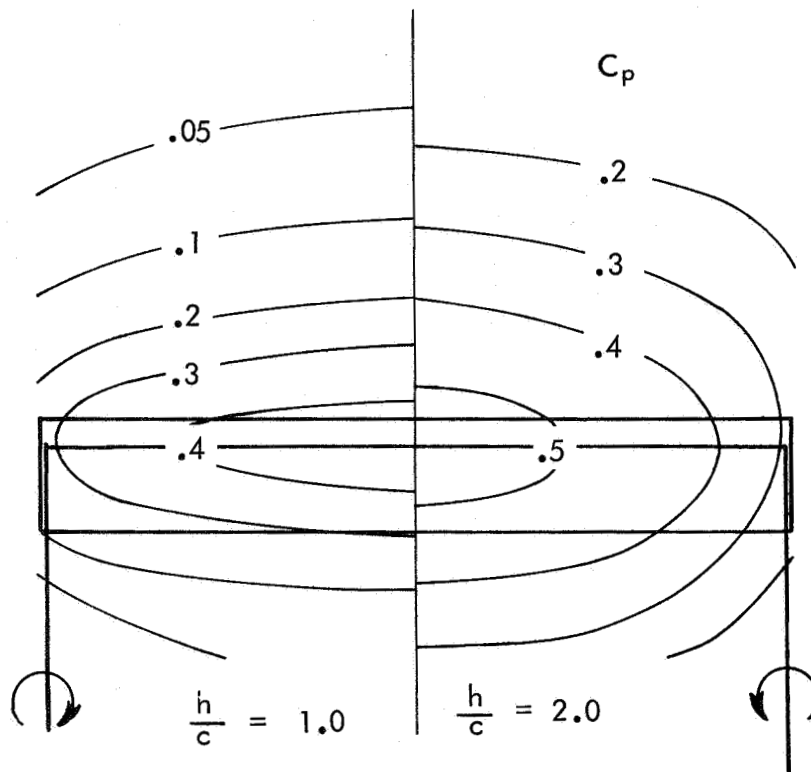
FIGURE 2. FLOOR PRESSURE CONTOURS FOR JET FLAP AND EXTERNALLY BLOWN FLAP CONFIGURATIONS



(i) C-130 Wing at $\frac{h}{c} = 1.66$ $C_L = 2.63$

$$\alpha = 12^\circ \quad \delta f = 25^\circ \quad \frac{C_f}{C} = .25$$

NO POWER APPLIED



$$C'_{L_{hb}} = 1.74 \quad C'_{L_{hb}} = 2.38$$

(ii) Simple Horseshoe Vortices

FIGURE 3. FLOOR PRESSURE CONTOURS FOR A C-130 WING AND A SIMPLE HORSESHOE VORTEX

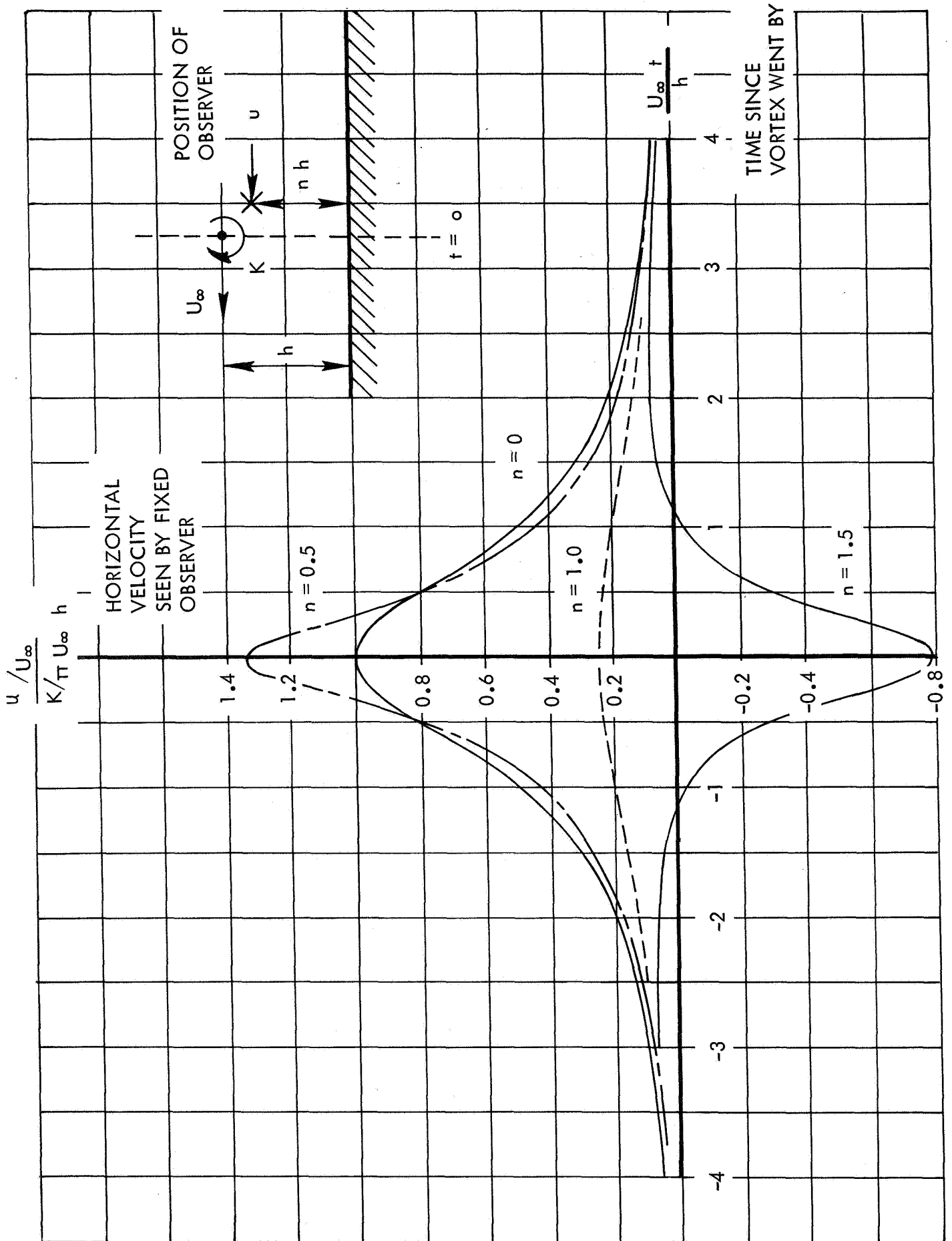


FIGURE 4. VELOCITY PAST A FIXED OBSERVER

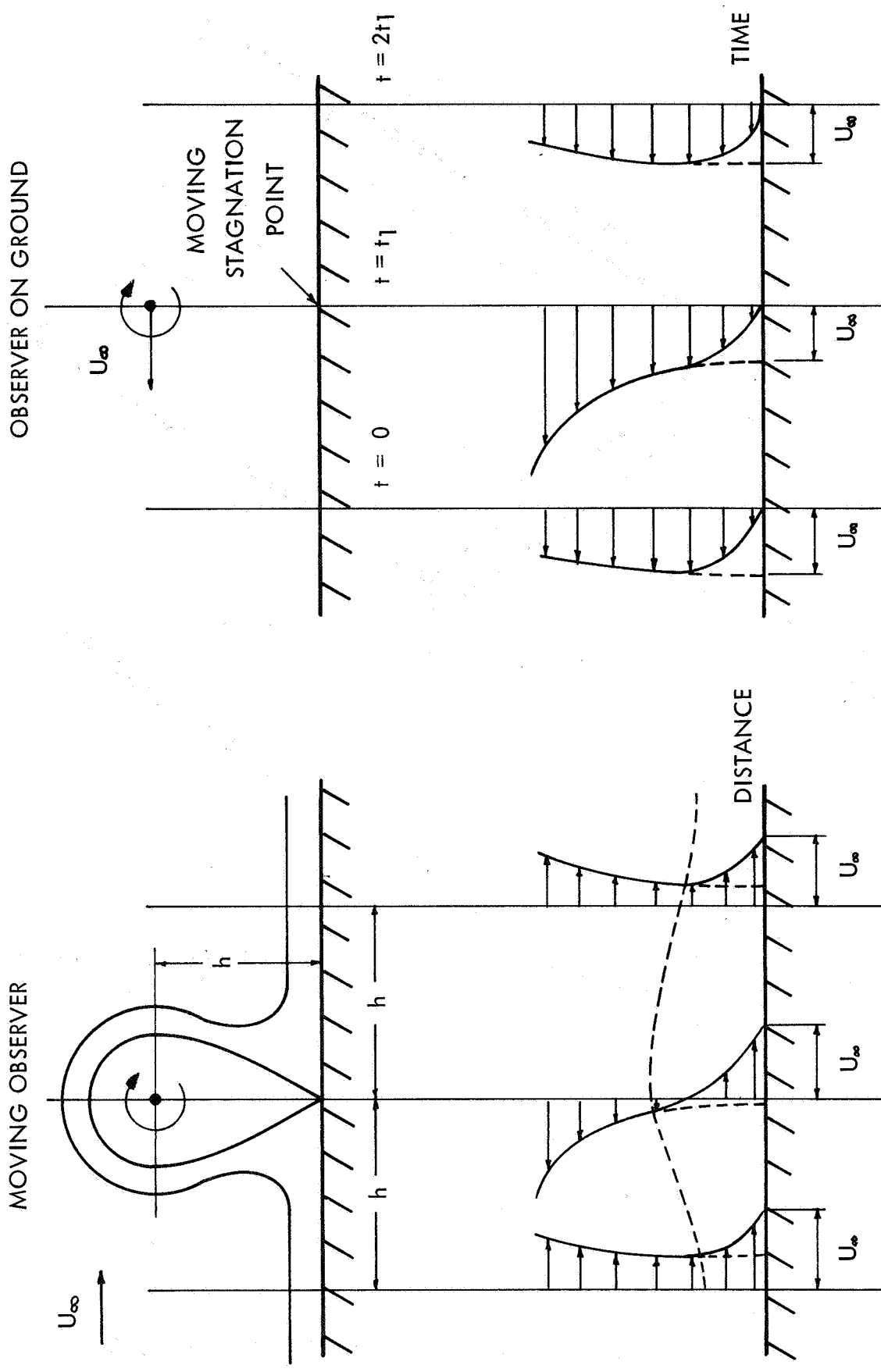


FIGURE 5. GROUND BOUNDARY LAYERS SEEN BY FIXED AND MOVING OBSERVERS

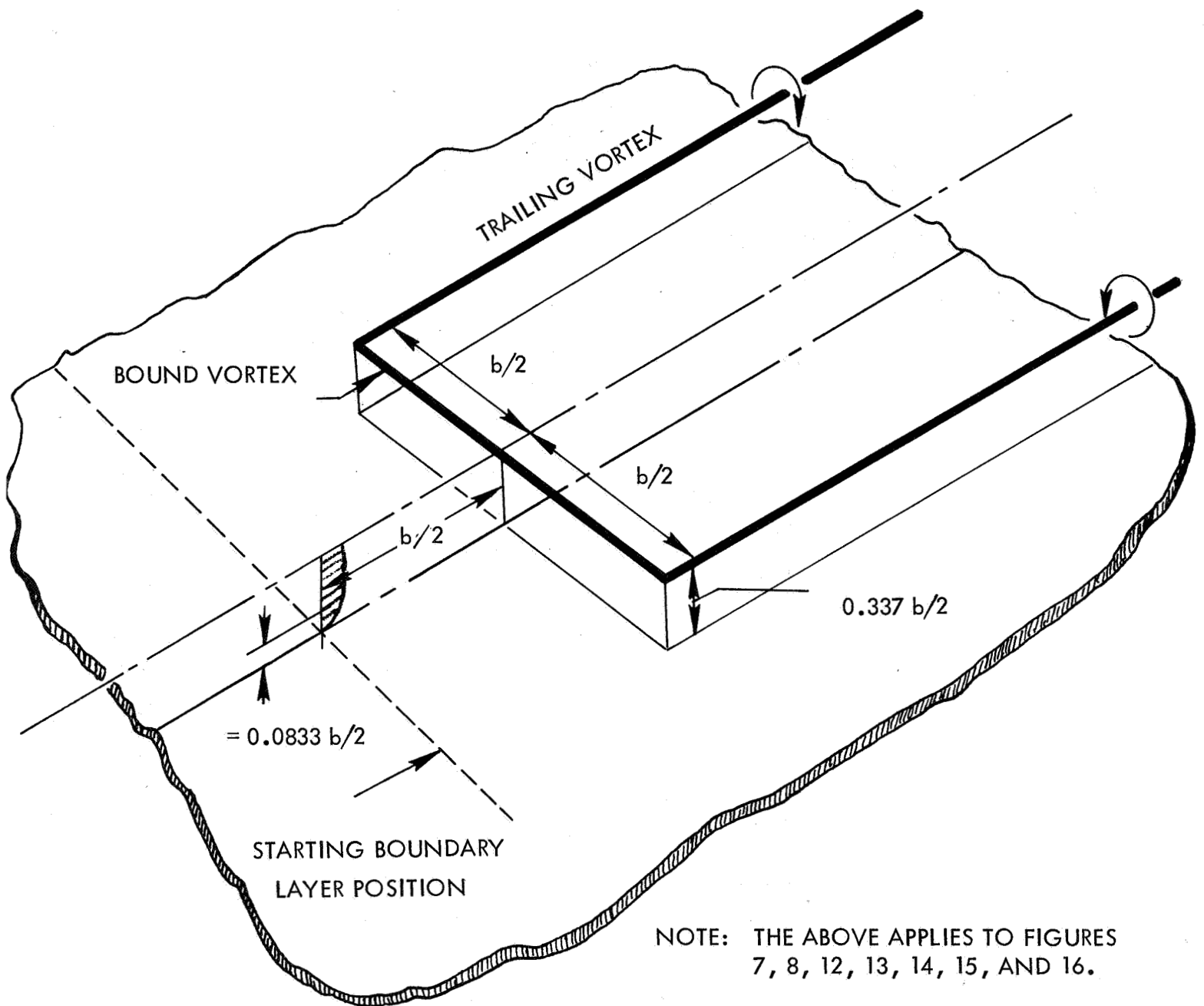


FIGURE 6. HORSESHOE VORTEX GEOMETRY FOR BOUNDARY LAYER STUDIES

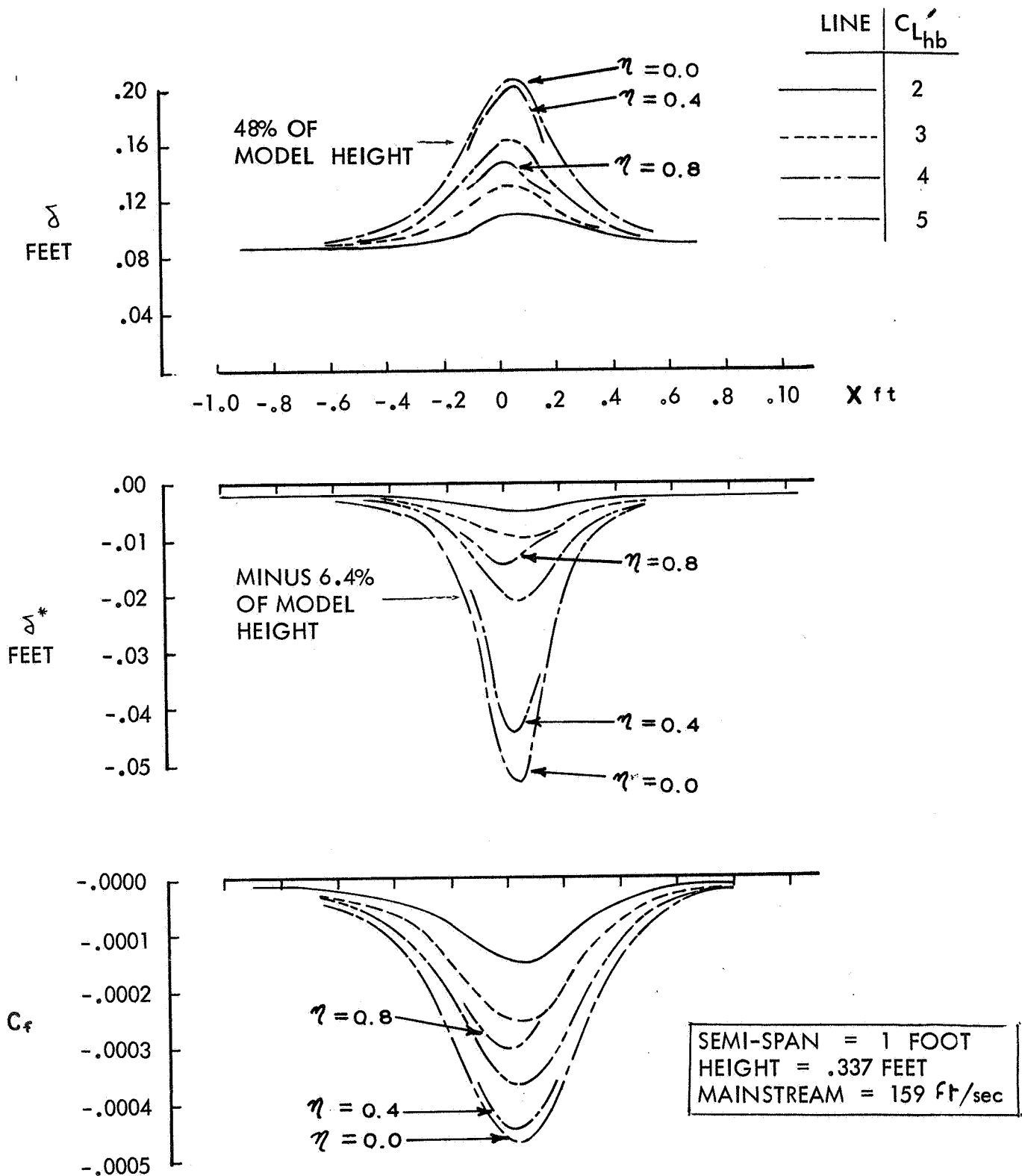


FIGURE 7. BOUNDARY LAYER THICKNESS AND WALL SHEAR STRESS:
LOW REYNOLDS NUMBER, MOVING GROUND.

NOTE: A CORRESPONDING FIXED GROUND CASE IS GIVEN IN FIGURE 13.

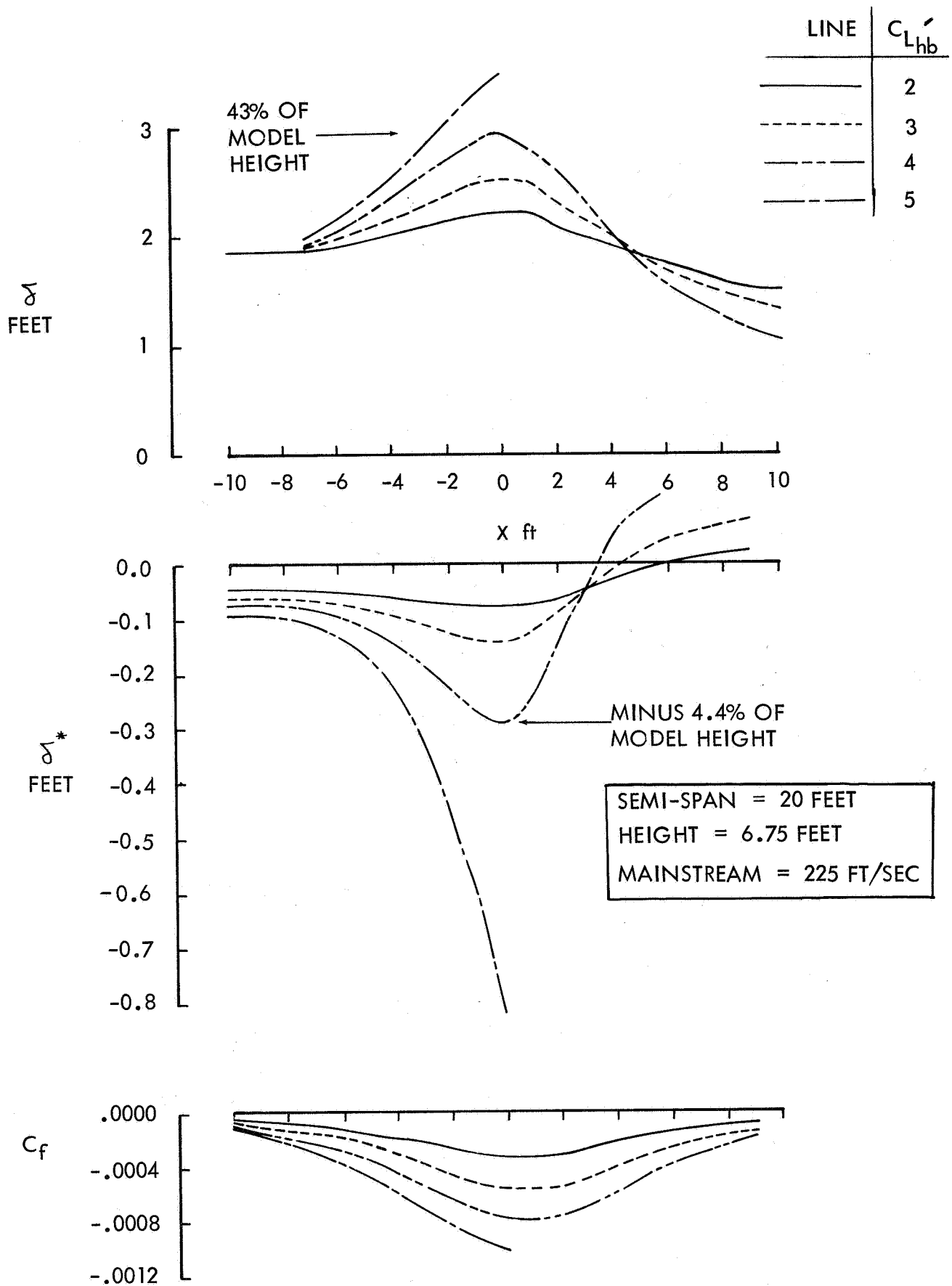


FIGURE 8. BOUNDARY LAYER THICKNESS AND WALL SHEAR STRESSES: HIGH REYNOLDS NUMBER, MOVING GROUND

NOTE: A CORRESPONDING FIXED GROUND CASE IS GIVEN IN FIGURE 4.

$$U_{\infty} = 96.0 \text{ FT/SEC}$$

$$Re_x = 610,000/\text{FT}$$

SYMBOL	$V_{\text{BELT}} \sim$	FT/SEC
○	0.0	
□	25.0	
△	50.0	

———— ROPER DATA (NASA TM X 2515)

----- NASH PROGRAM - ROUGH BELT

- - - - NASH PROGRAM - SMOOTH BELT

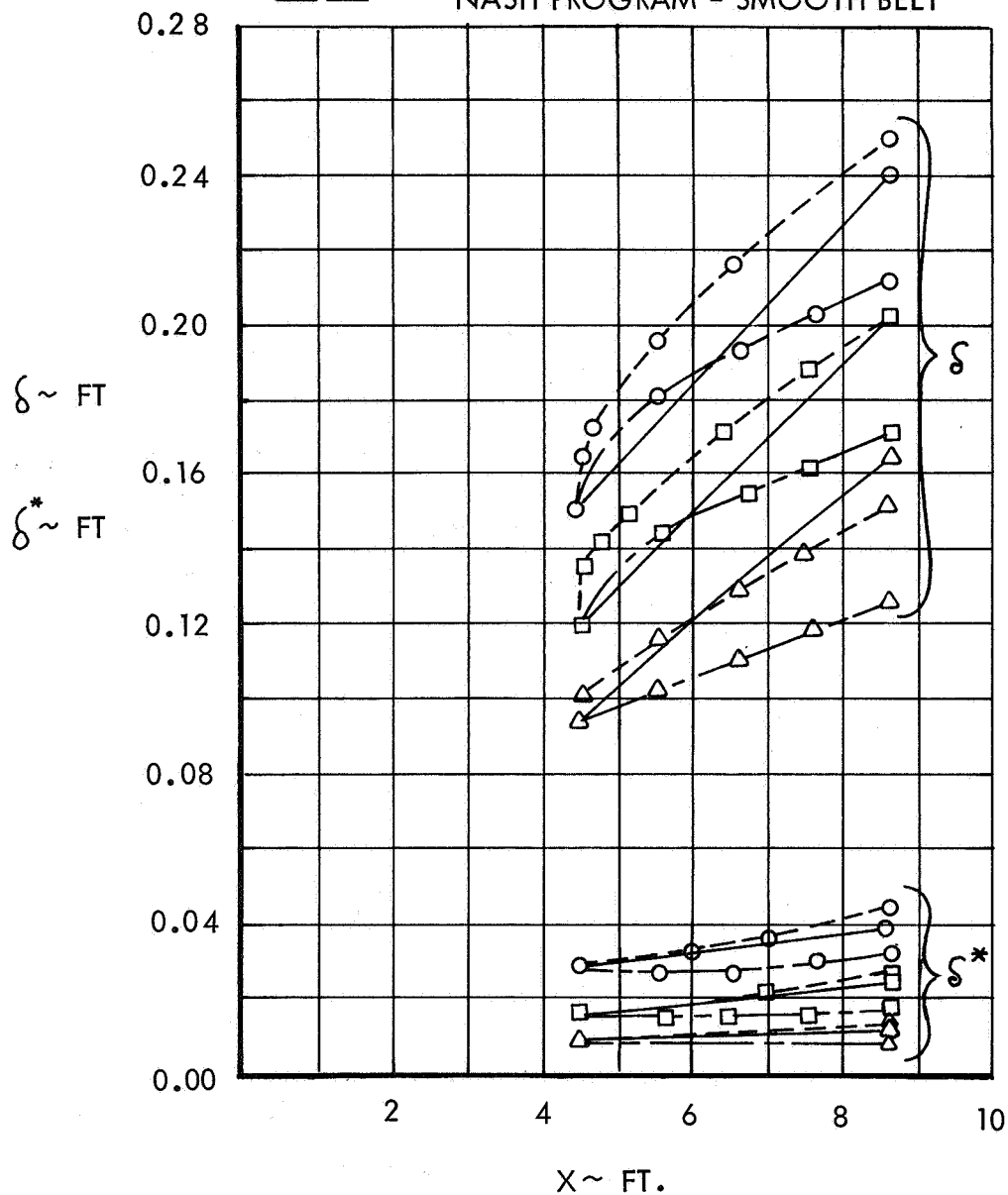


FIGURE 9. MOVING GROUND BOUNDARY LAYER CORRELATION:
(i) BOUNDARY LAYER GROWTH

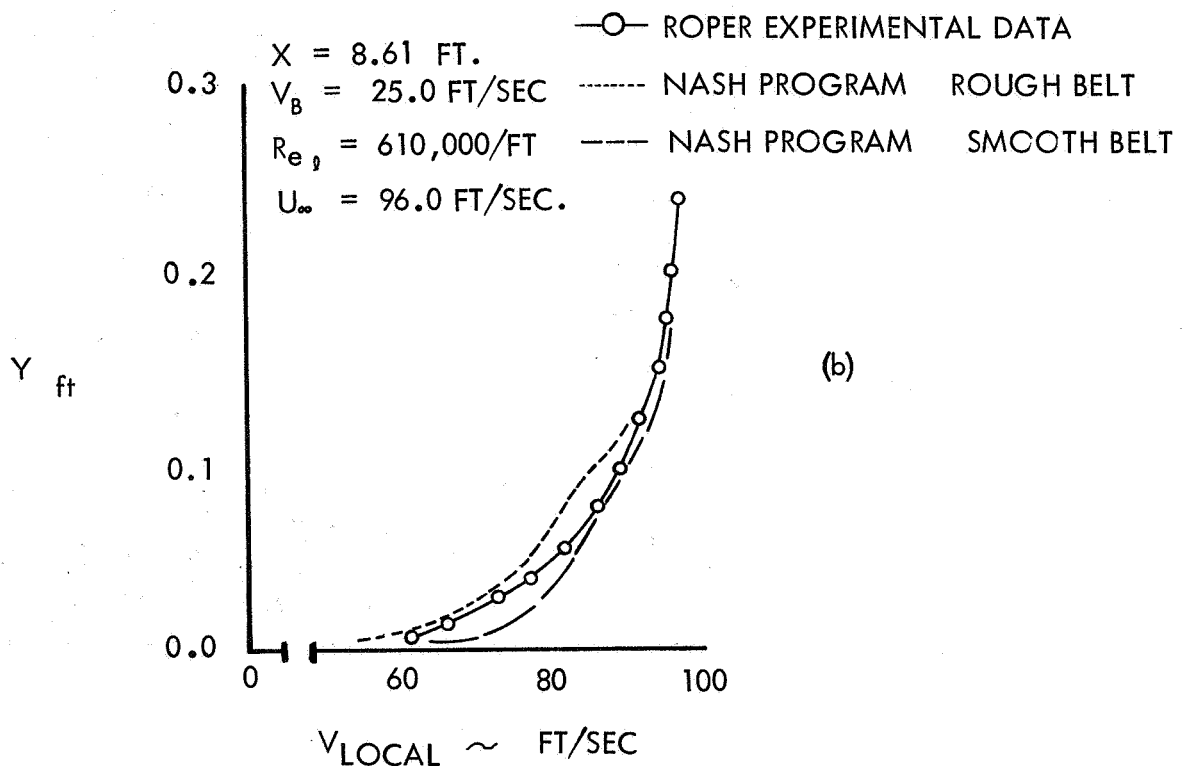
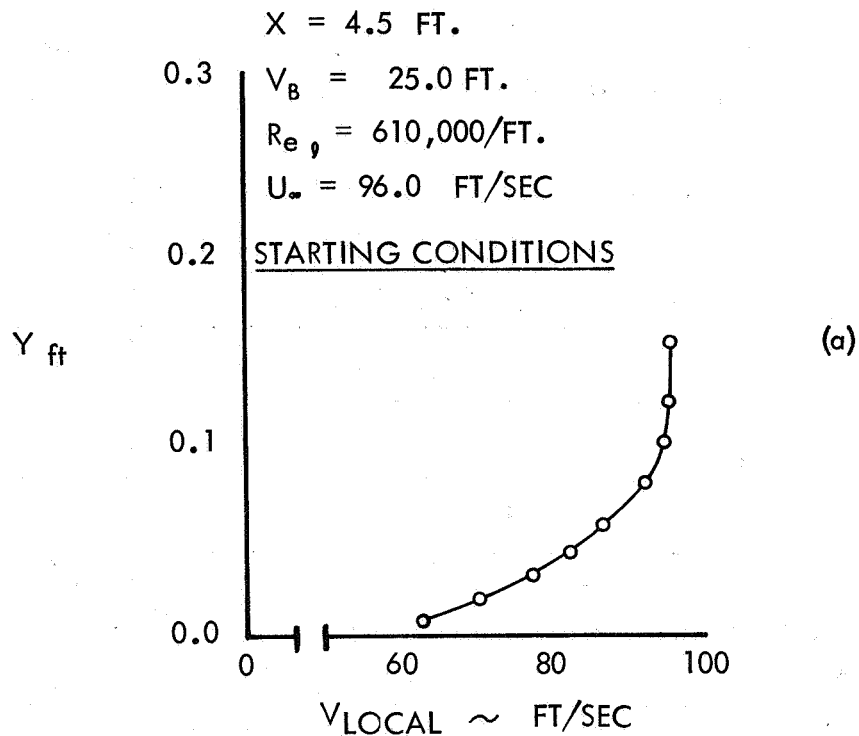


FIGURE 10. MOVING GROUND BOUNDARY LAYER CORRELATION:
 (ii) BOUNDARY LAYER PROFILES FOR $V_B/V_\infty = .25$

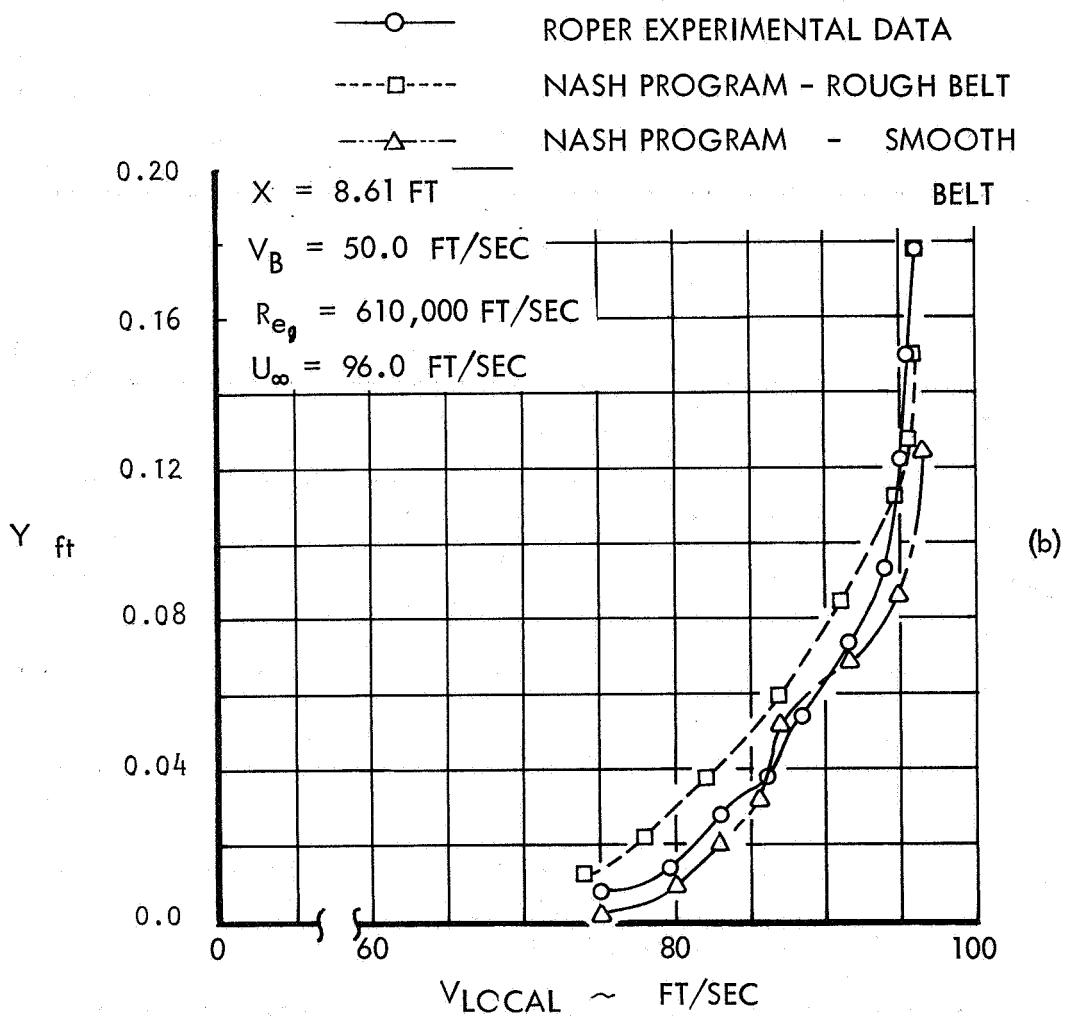
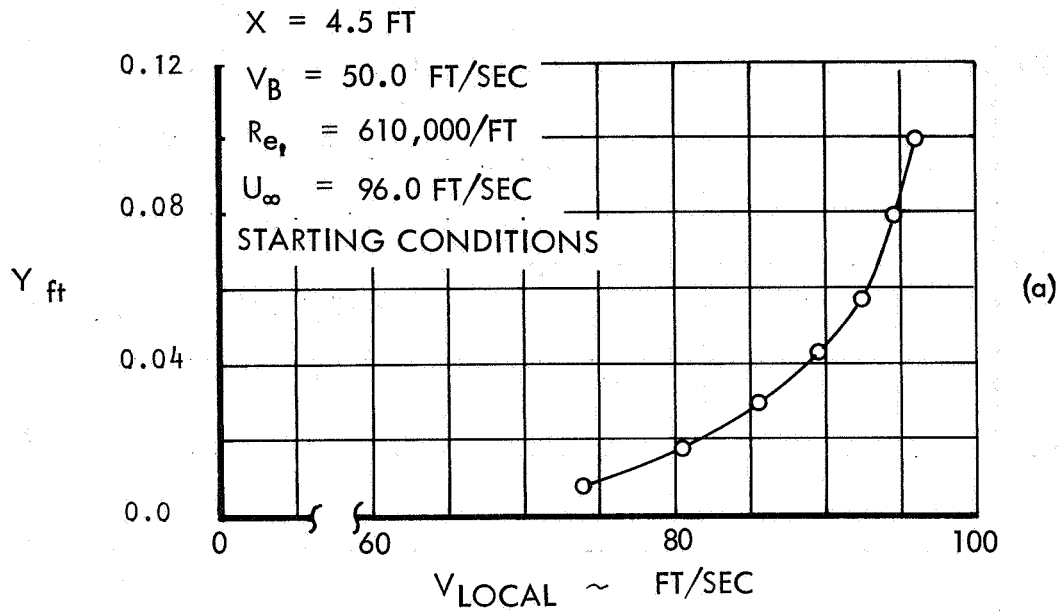


FIGURE 11. MOVING GROUND BOUNDARY LAYER CORRELATIONS
 (ii) BOUNDARY LAYER PROFILE FOR $V_B/V_\infty = .50$

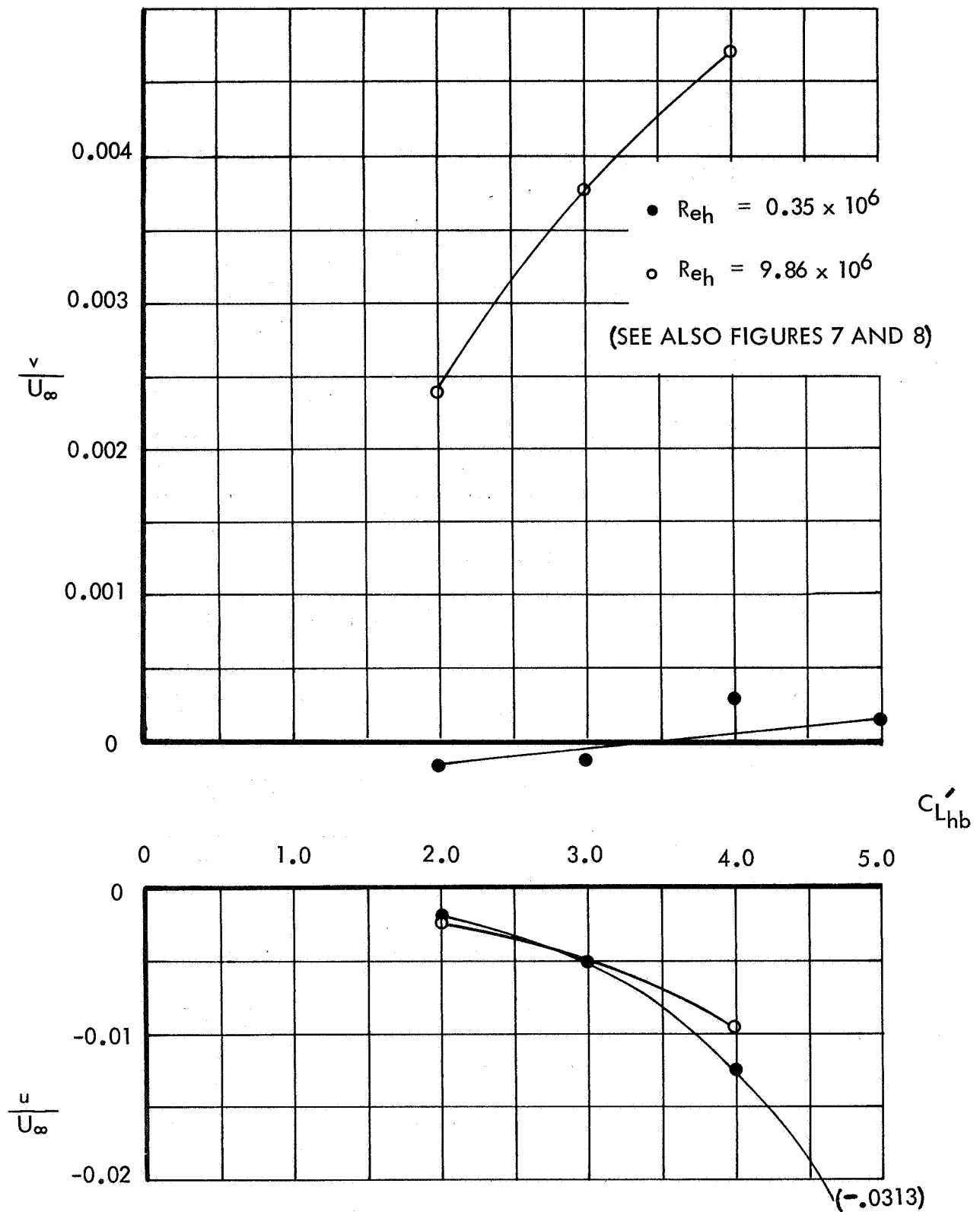
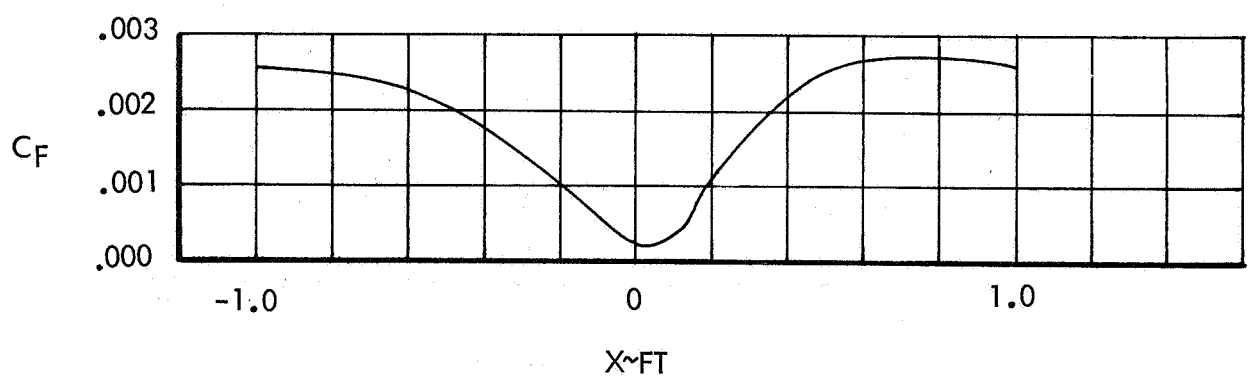
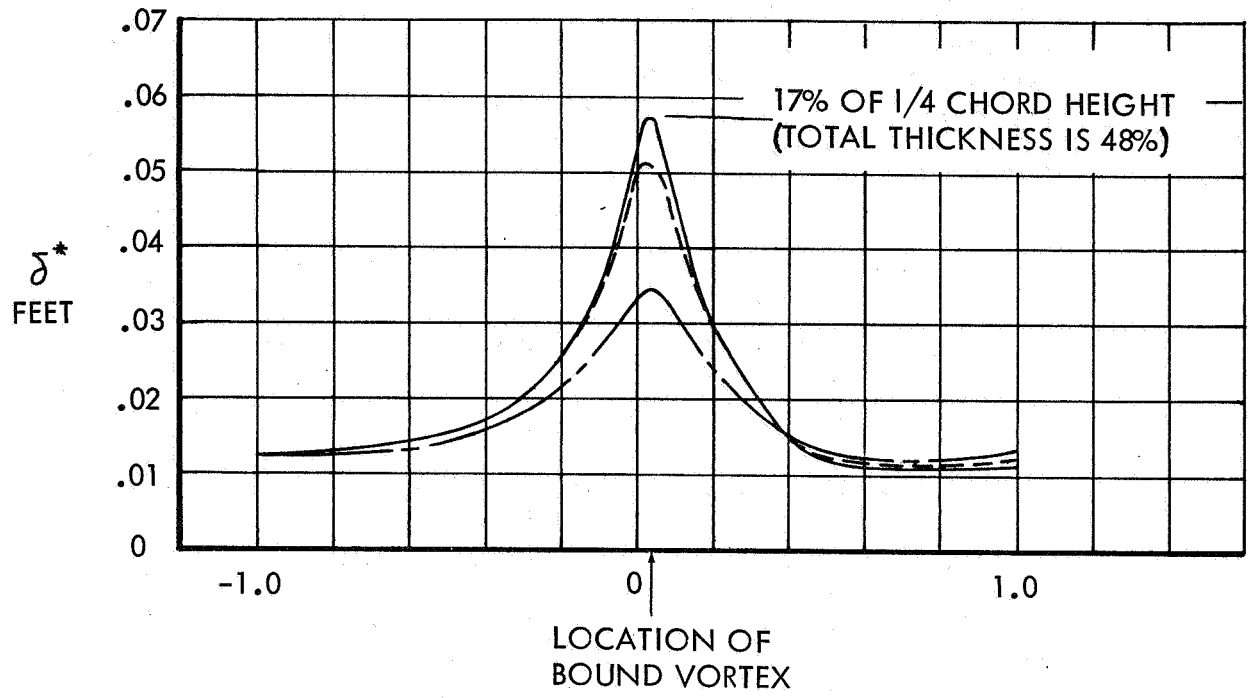


FIGURE 12 INDUCED FLOW, AT THE CENTER OF THE BOUND VORTEX, CAUSED BY ENTRAINMENT INTO A MOVING-GROUND BOUNDARY LAYER

NOTE: THE CORRESPONDING FIXED-GROUND AND WALL-JET PLOTS ARE GIVEN IN FIGURES 16 AND 25, RESPECTIVELY.



SEMISPAN = 1 FOOT = λ
 HEIGHT = 0.337 FEET
 MAINSTREAM = 159 FT/SEC.
 $C_{L_{hb}}' = 1.74$ (= .95 OF SEPARATION VALUE)

LEGEND: η
 ————— 0.0
 - - - - - +0.4
 - · - · - · - 0.8

FIGURE 13 BOUNDARY LAYER THICKNESS AND WALL SHEAR STRESS:
 LOW REYNOLDS NUMBER, FIXED GROUND ($Re_\lambda = 1.019 \times 10^6$)

NOTE: THE CORRESPONDING MOVING GROUND PLOTS ARE GIVEN IN FIGURE 7.

SEMISPAN = 20 FEET = l
 HEIGHT = 6.75 FEET
 MAINSTREAM = 225 FT/SEC
 $C_{L_{hb}} = 1.74$ (= 74% OF SEPARATION VALUE)

LEGEND : η
 ————— 0.0
 - - - - - ± 0.4
 - · - · - ± 0.8

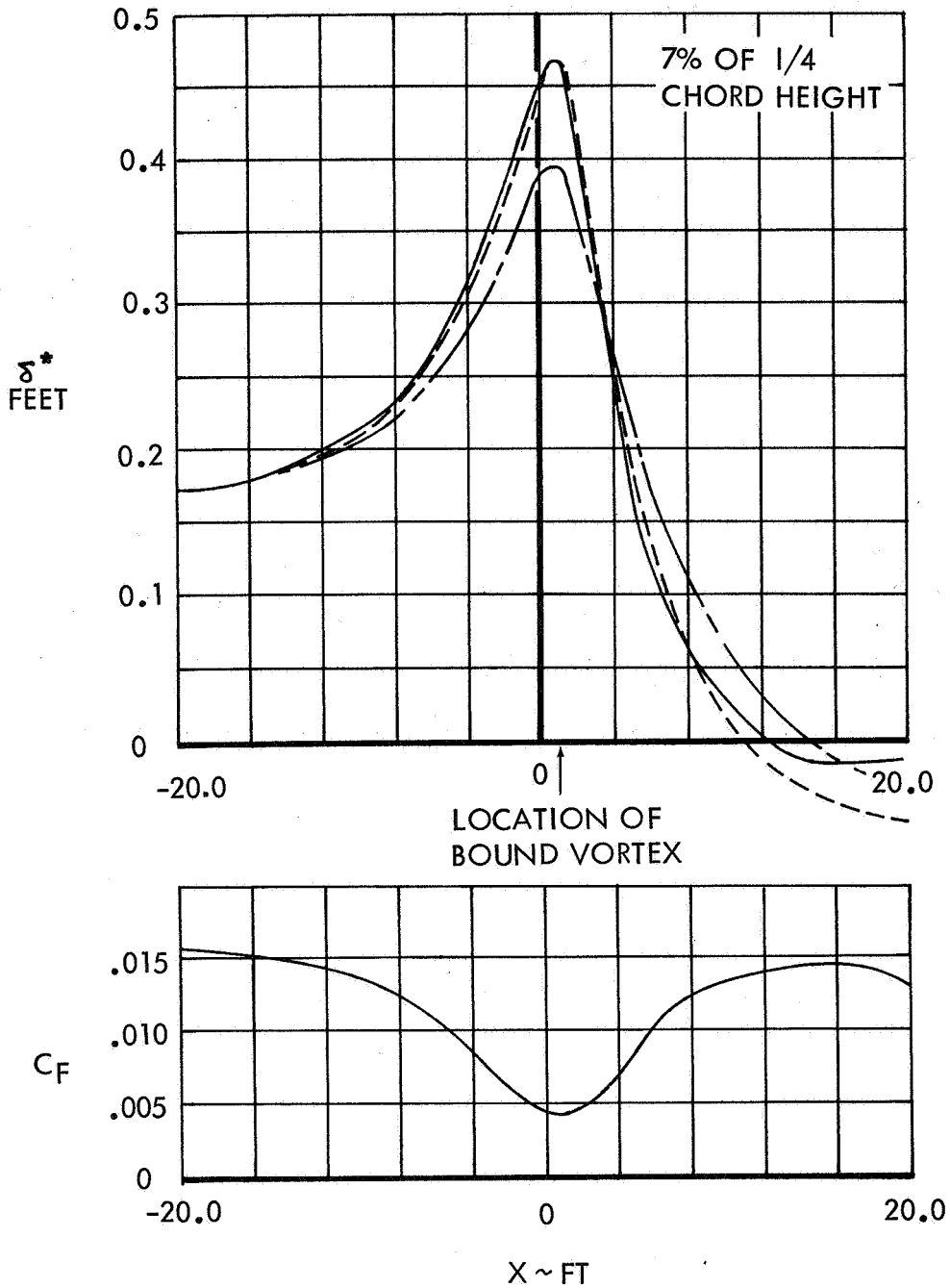


FIGURE 14 BOUNDARY LAYER THICKNESS AND WALL SHEAR STRESS
 HIGH REYNOLDS NUMBER, FIXED GROUND ($Re_l = 28.8 \times 10^6$)

NOTE: THE CORRESPONDING MOVING GROUND PLOTS ARE GIVEN IN FIGURE 8.

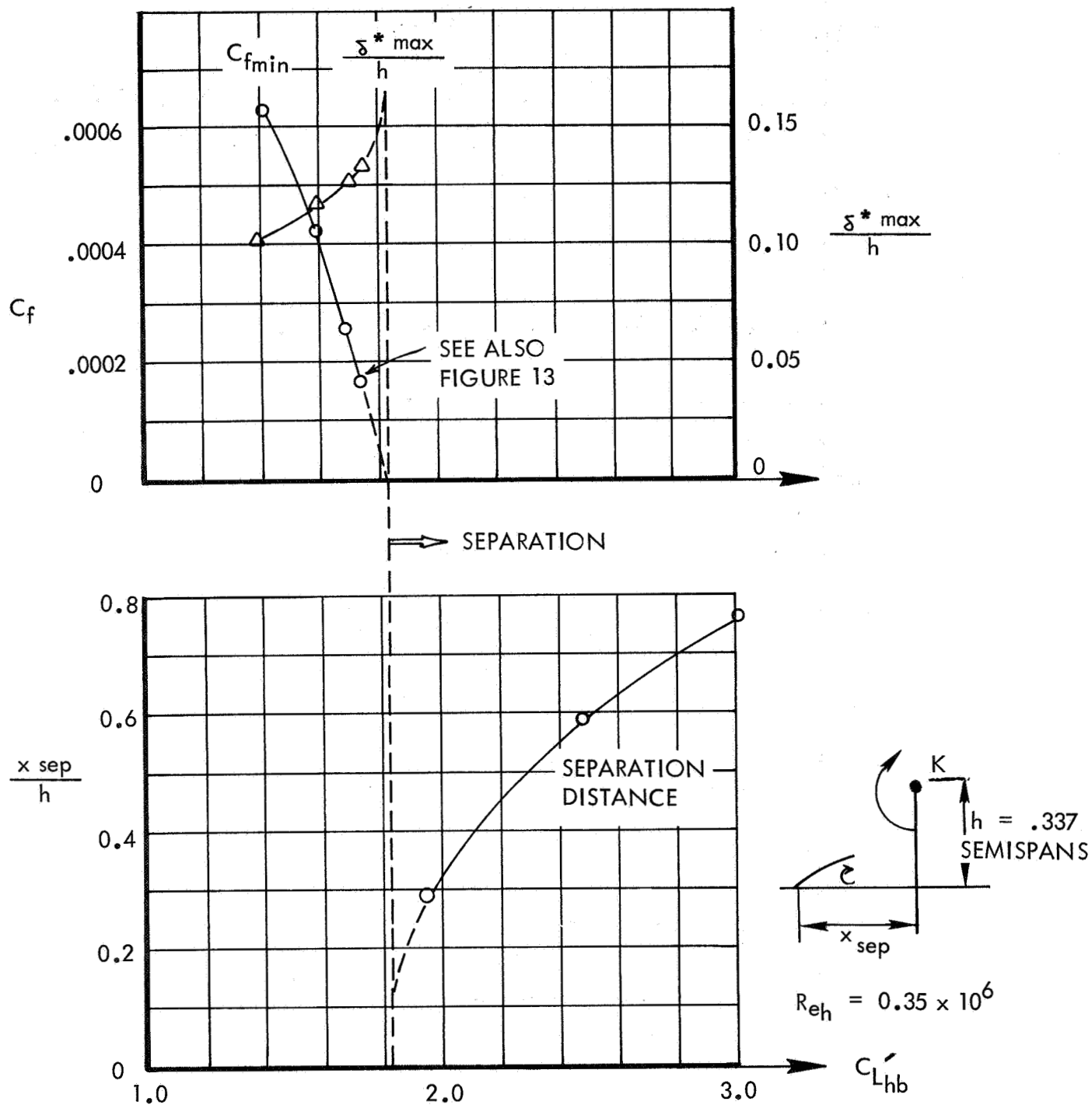


FIGURE 15 SEPARATION OF FIXED GROUND BOUNDARY LAYER FOR A UNIFORMLY-LOADED, FINITE, UNIT SEMISPAN WING

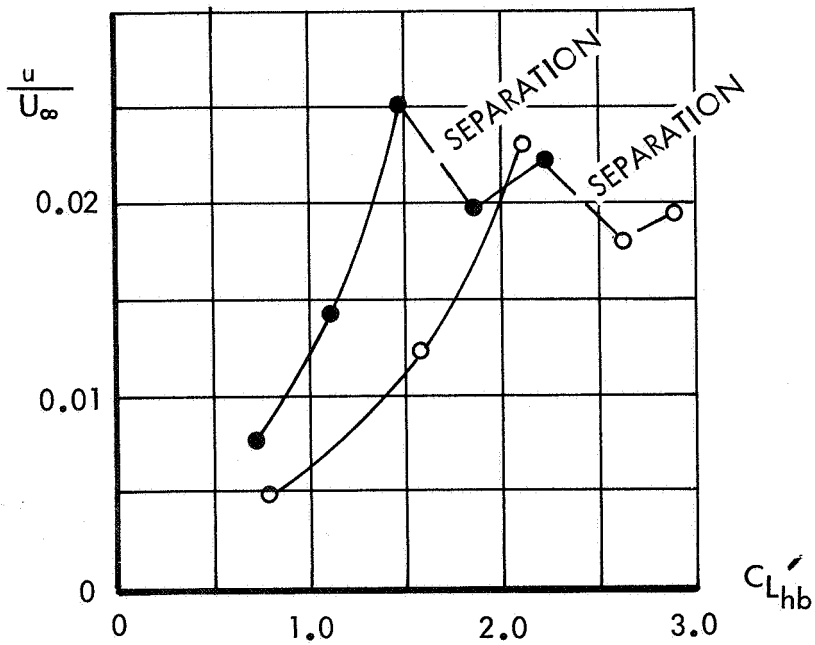
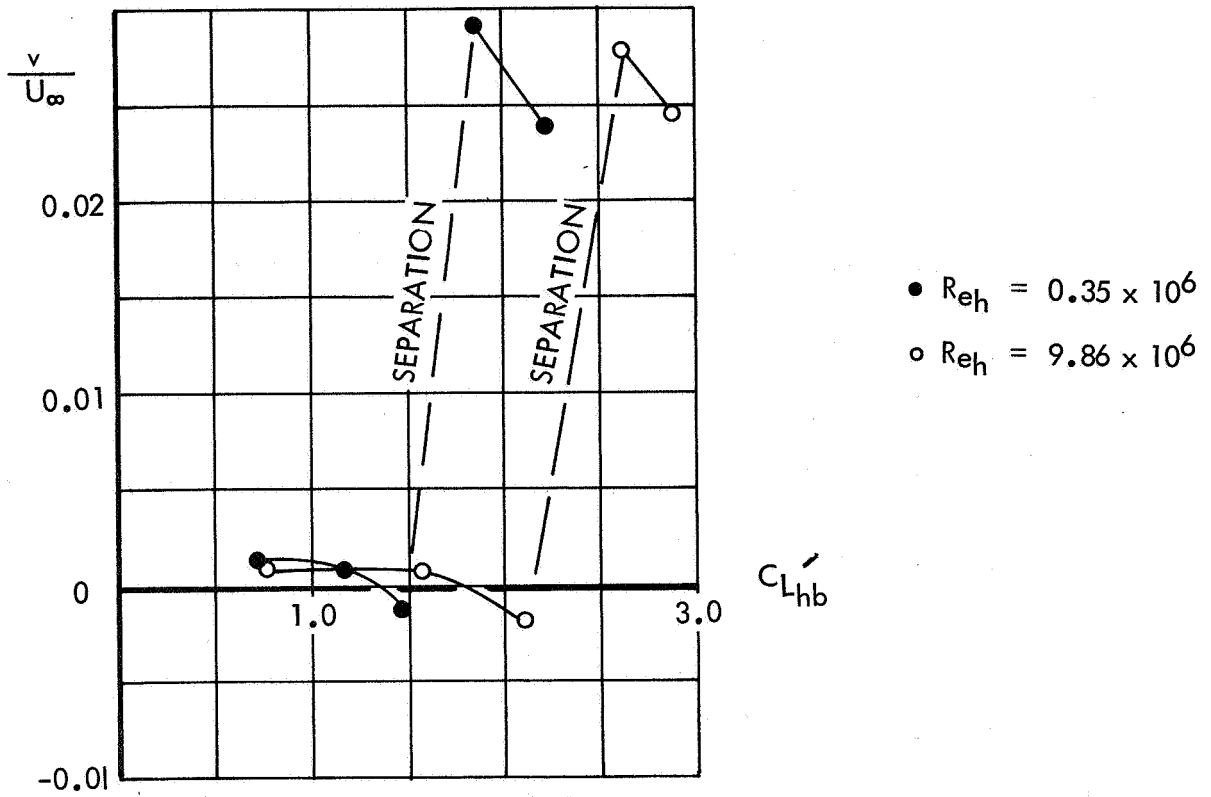


FIGURE 16 INDUCED FLOW, AT THE CENTER OF THE BOUND VORTEX, CAUSED BY ENTRAINMENT INTO A FIXED-GROUND BOUNDARY-LAYER

NOTE: THE CORRESPONDING MOVING GROUND AND WALL JET PLOTS ARE GIVEN IN FIGURES 12 AND 25, RESPECTIVELY.

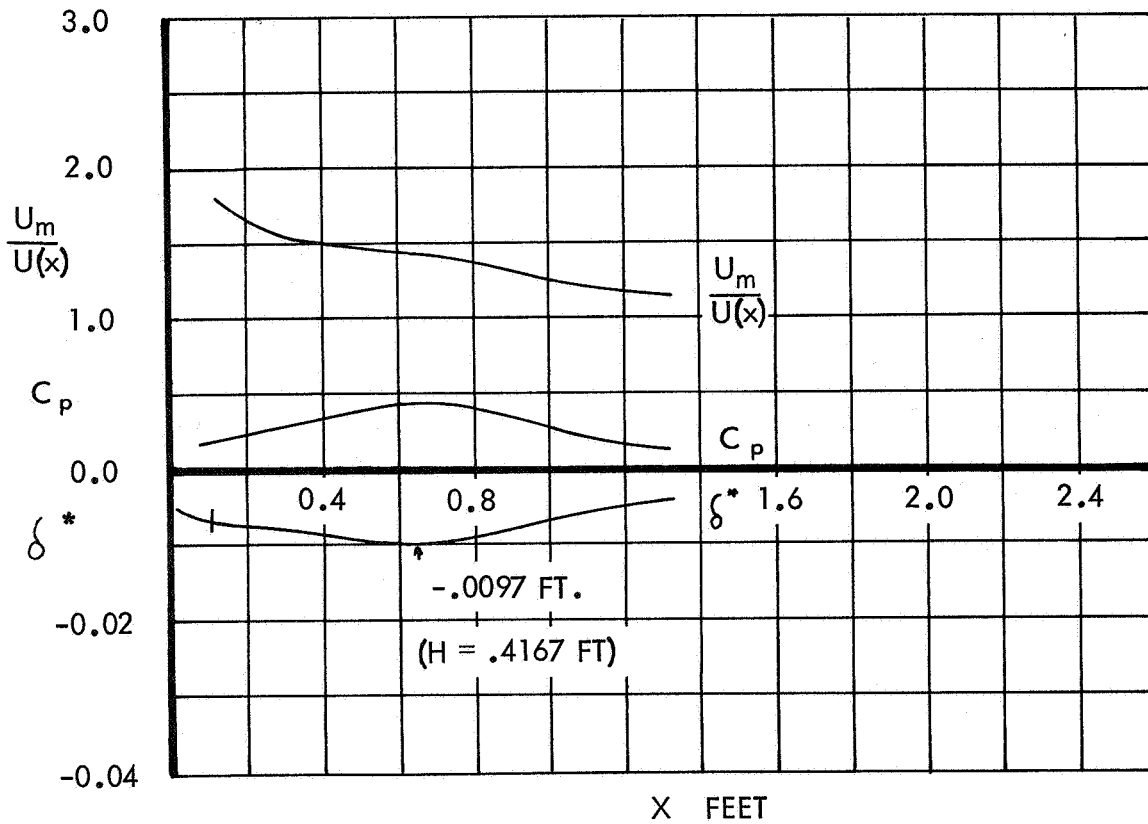
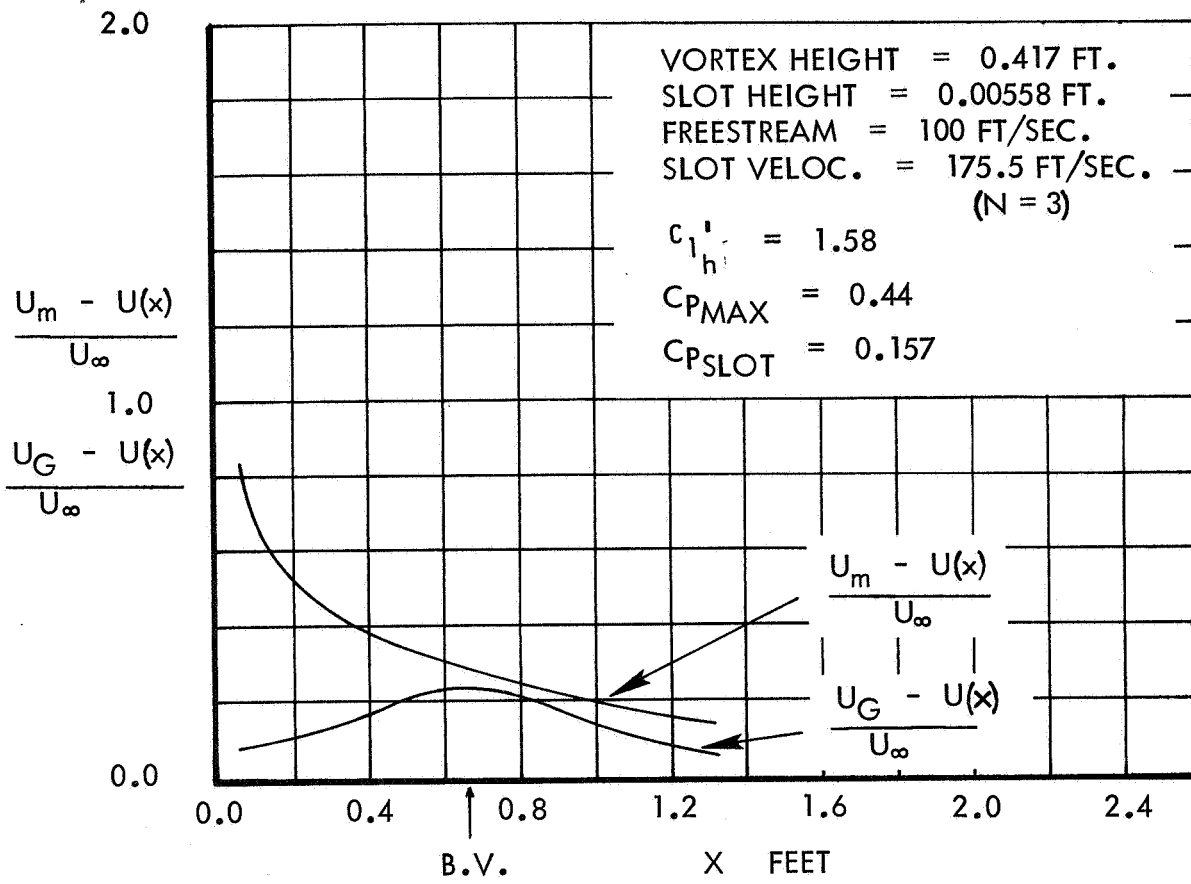


FIGURE 18 BASE CASE FOR EARLY WALL JET THEORETICAL STUDIES, $c_{1h}^i = 1.58$

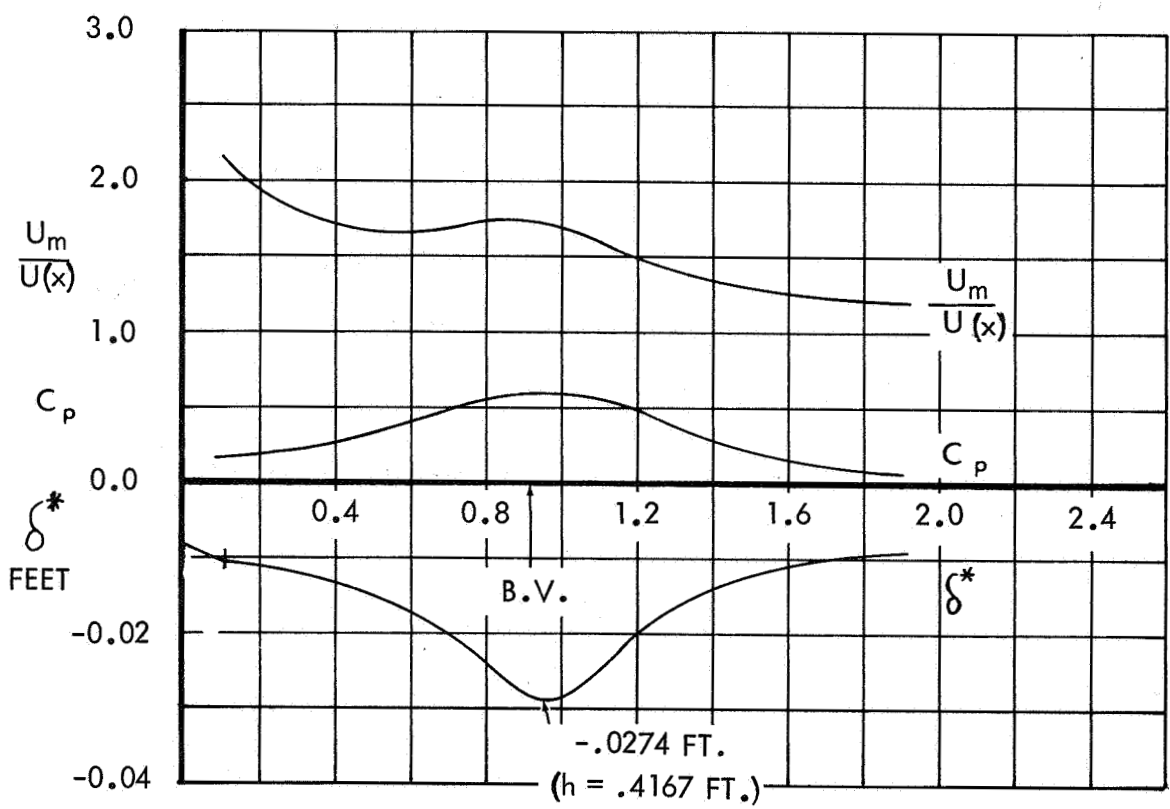
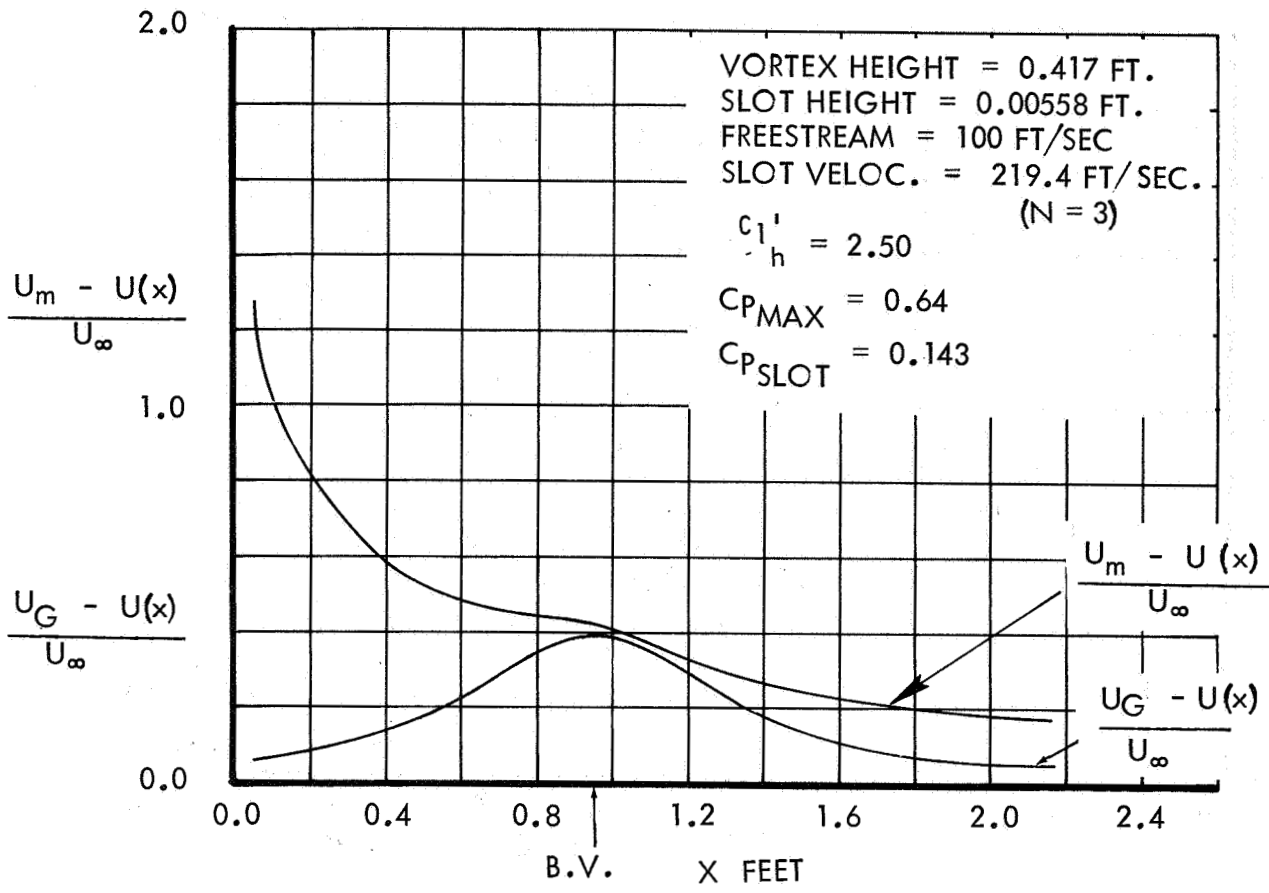


FIGURE 19 WALL JET DECAY ON GROUND, $c_{1h}' = 2.50$

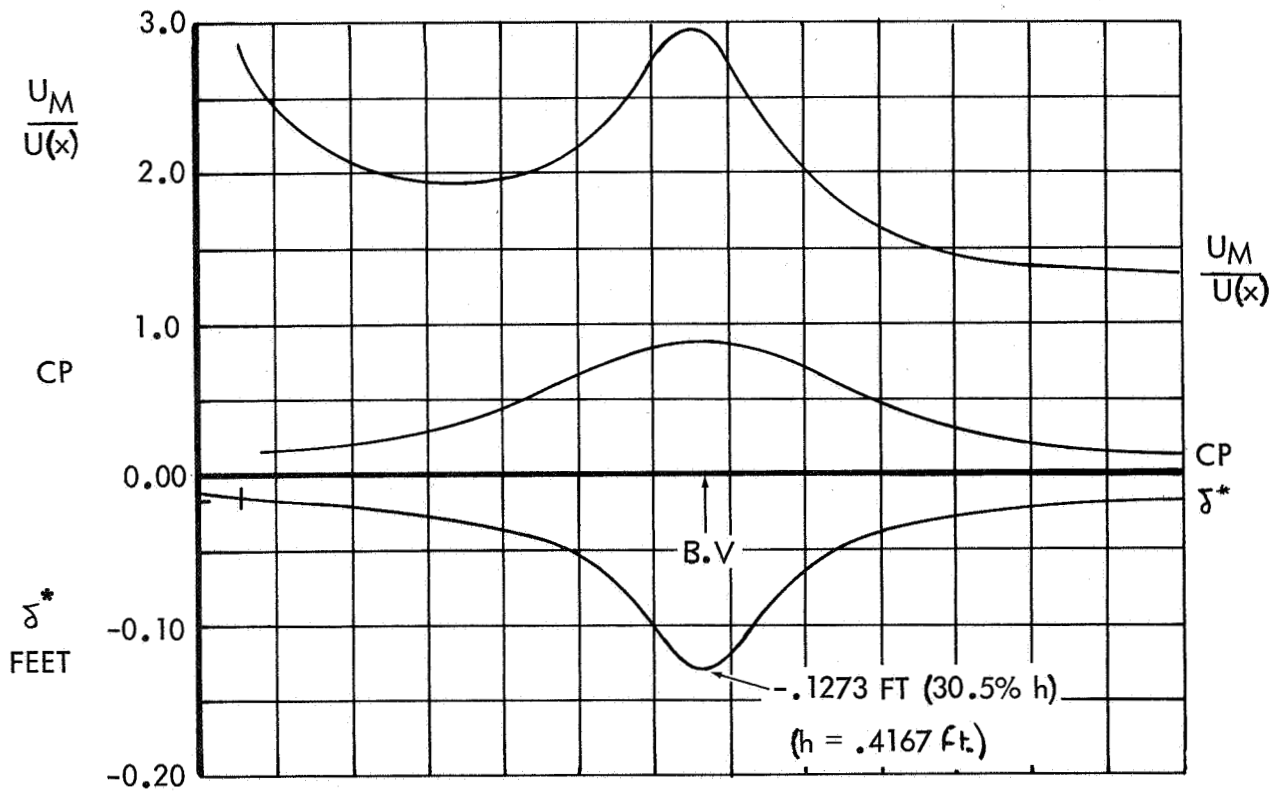
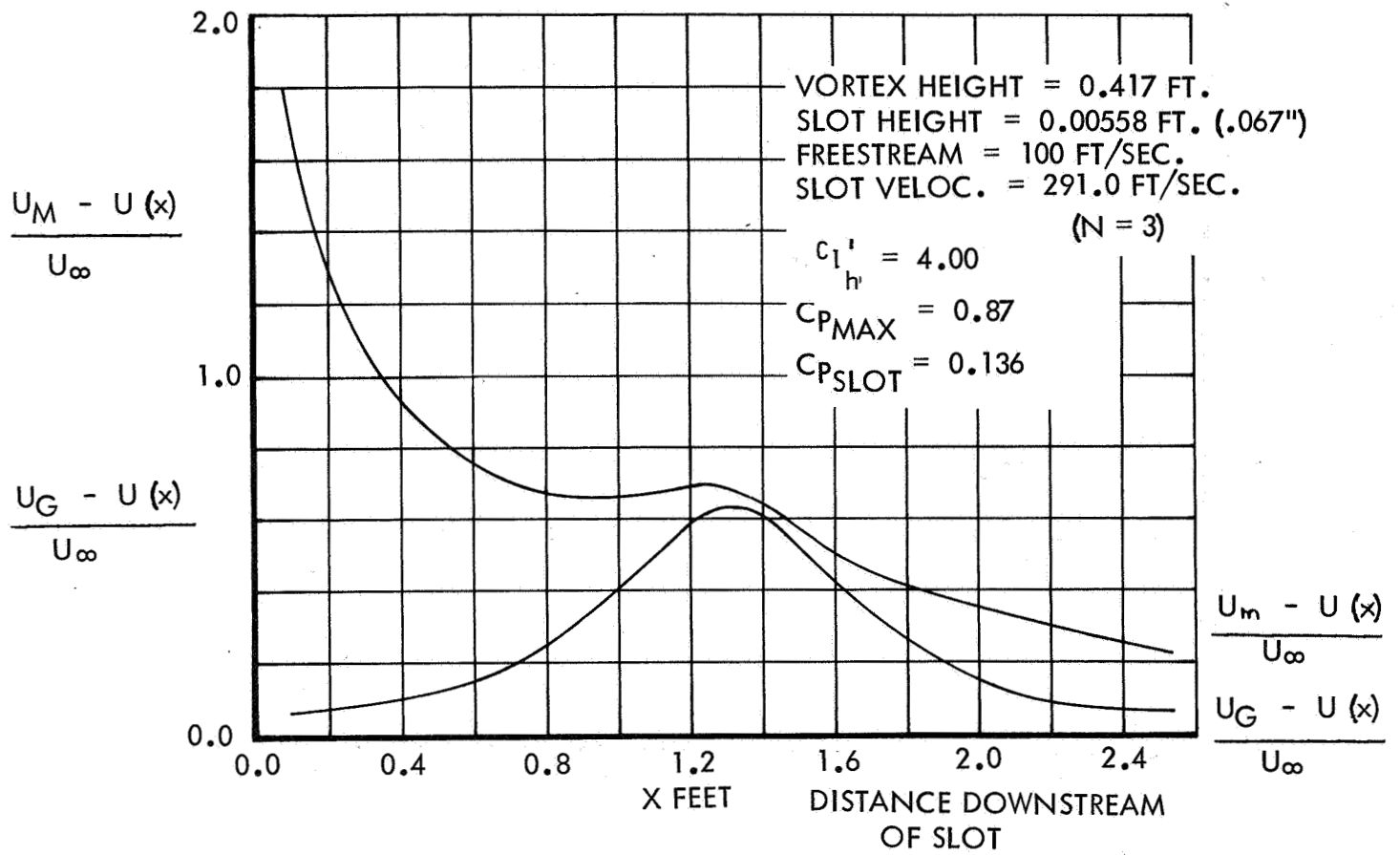
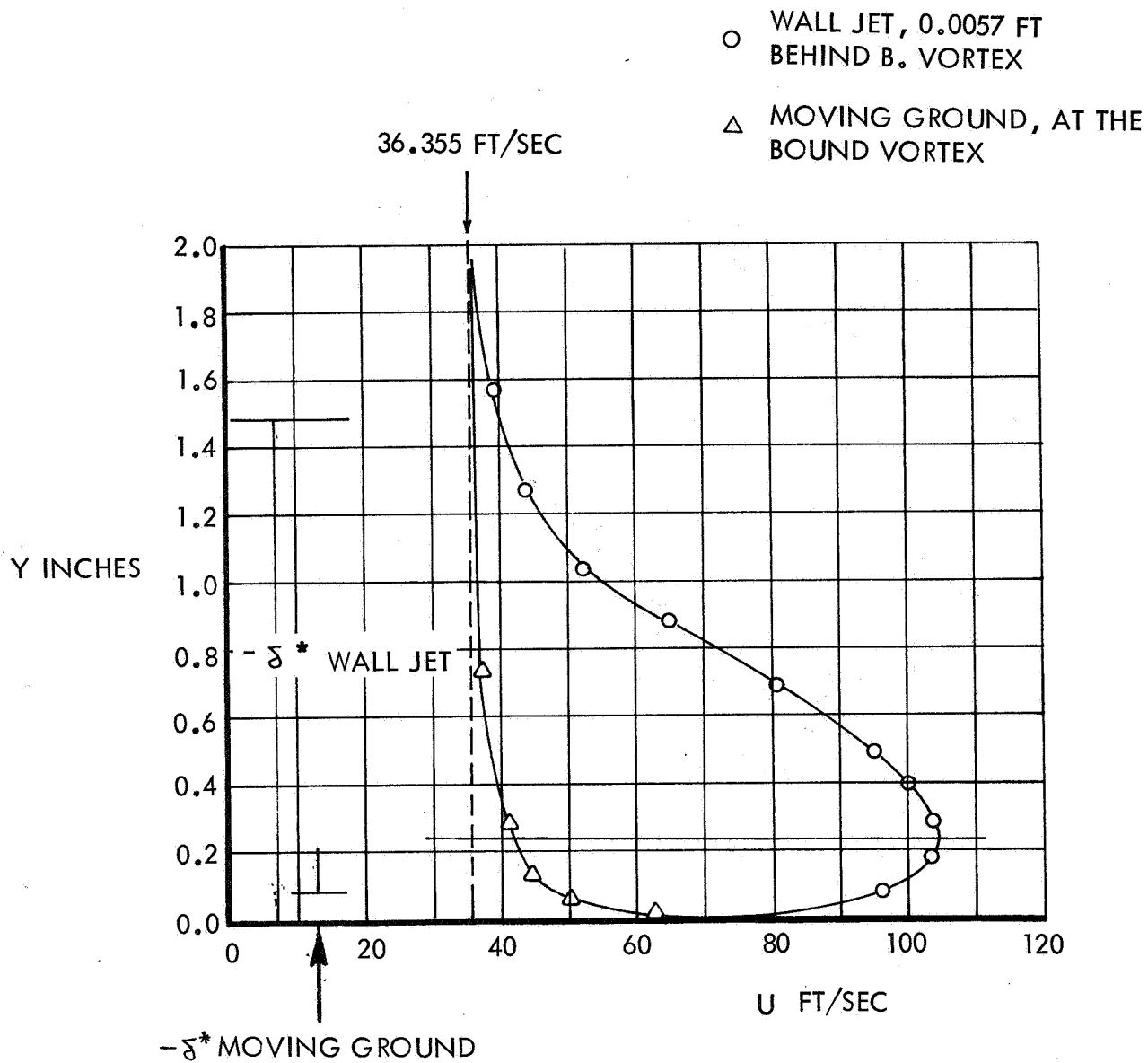


FIGURE 20 WALL JET DECAY ON GROUND, $c_{1h} = 4.0$



WALL JET $\delta^* = -0.1220$ FT.
 MOVING GROUND $\delta^* = -0.007454$ FT.

FIGURE 21 MOVING GROUND AND WALL JET VELOCITY PROFILES
 AT BOUND VORTEX POSITION, $c_{1h} = 4.00$

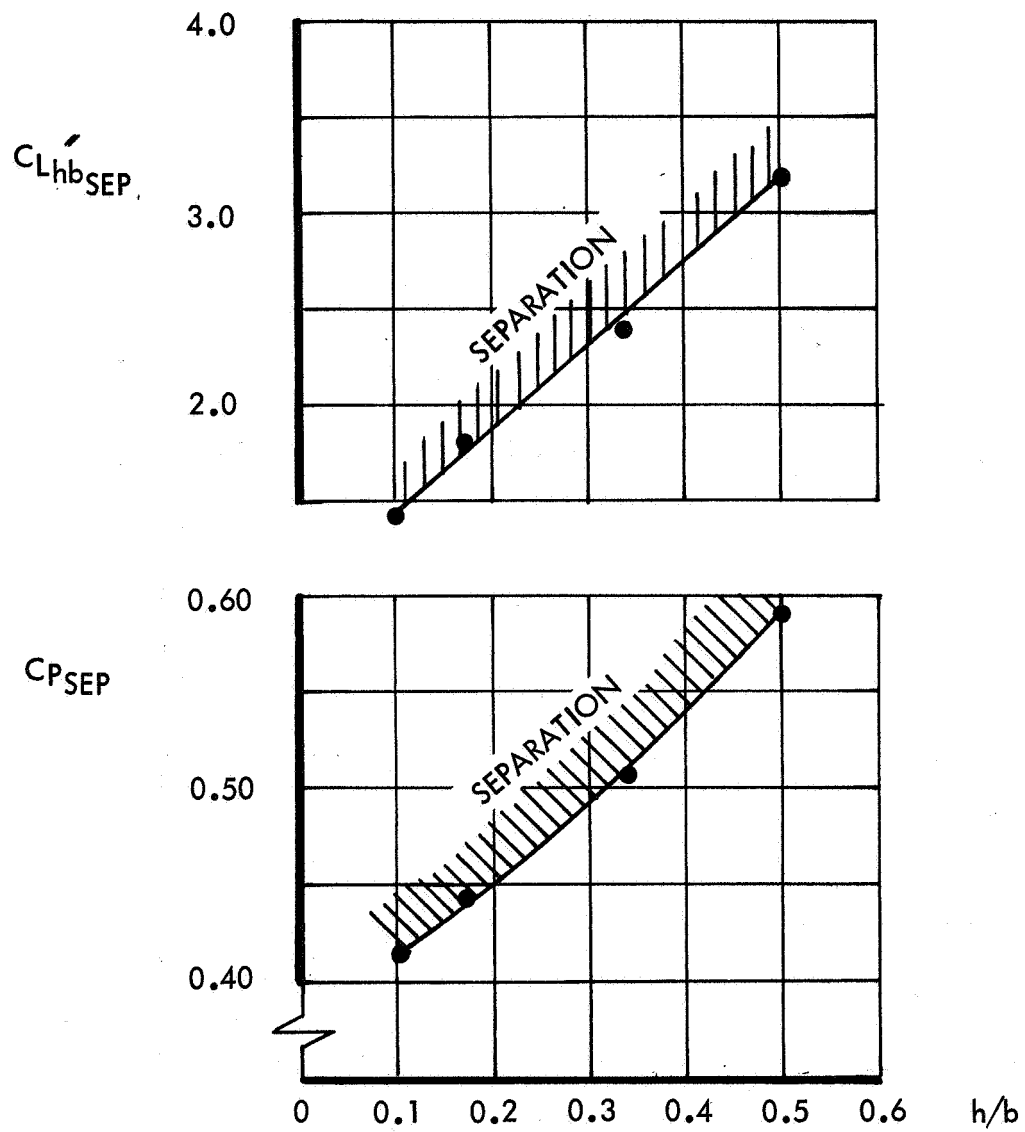
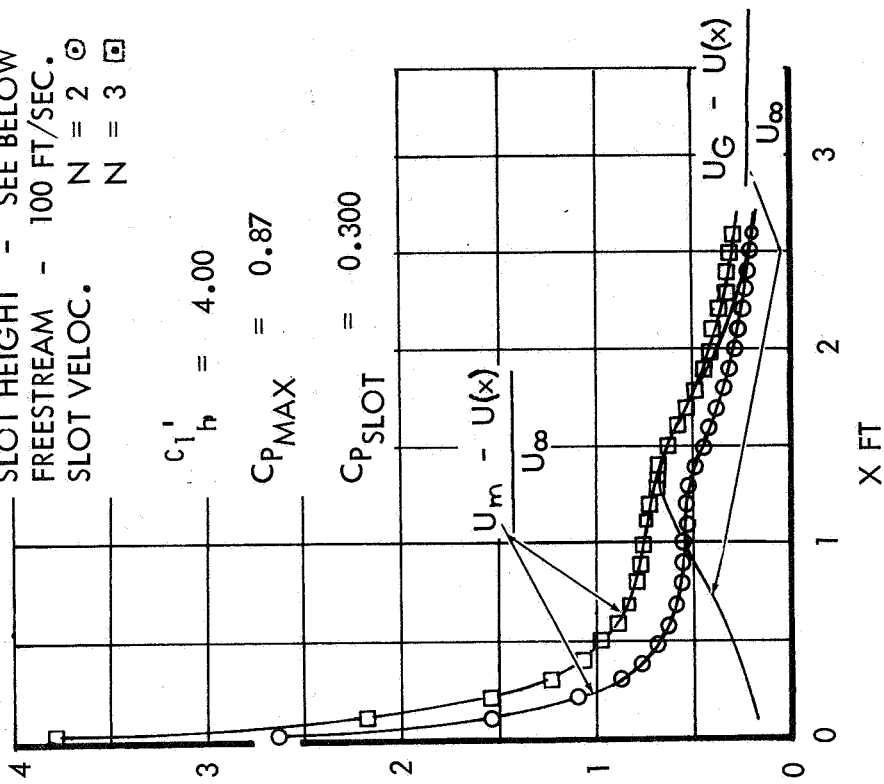


FIGURE 22 THEORETICAL FLOOR SEPARATION CRITERIA, IN THREE DIMENSIONS, FOR A SIMPLE HORSESHOE VORTEX AT LOW REYNOLDS NUMBER

VORTEX HEIGHT = 0.768 FT.
 SLOT HEIGHT - SEE BELOW
 FREESTREAM - 100 FT/SEC.
 SLOT VELOC. N = 2 ⊙
 N = 3 ⊠

$c_{1h}' = 4.00$
 $C_{P_{MAX}} = 0.87$
 $C_{P_{SLOT}} = 0.300$



H_SLOT = 0.0056 FT (0.067")
 227.1 FT/SEC. (N = 2)
 291.0 FT/SEC. (N = 3)

(a)

H_SLOT = 0.0022 FT (0.026")
 359.6 FT/SEC. (N = 4.08)
 462.0 FT/SEC. (N = 5.69)

(b)

} SAME THRUST AS (a)

FIGURE 23 EFFECT OF SLOT HEIGHT - LOW REYNOLDS NUMBER

VORTEX HEIGHT = 9.222 FT

SLOT HEIGHT - SEE BELOW

FREESTREAM VELOC 152 FT/SEC

SLOT VELOC N = 2 ○

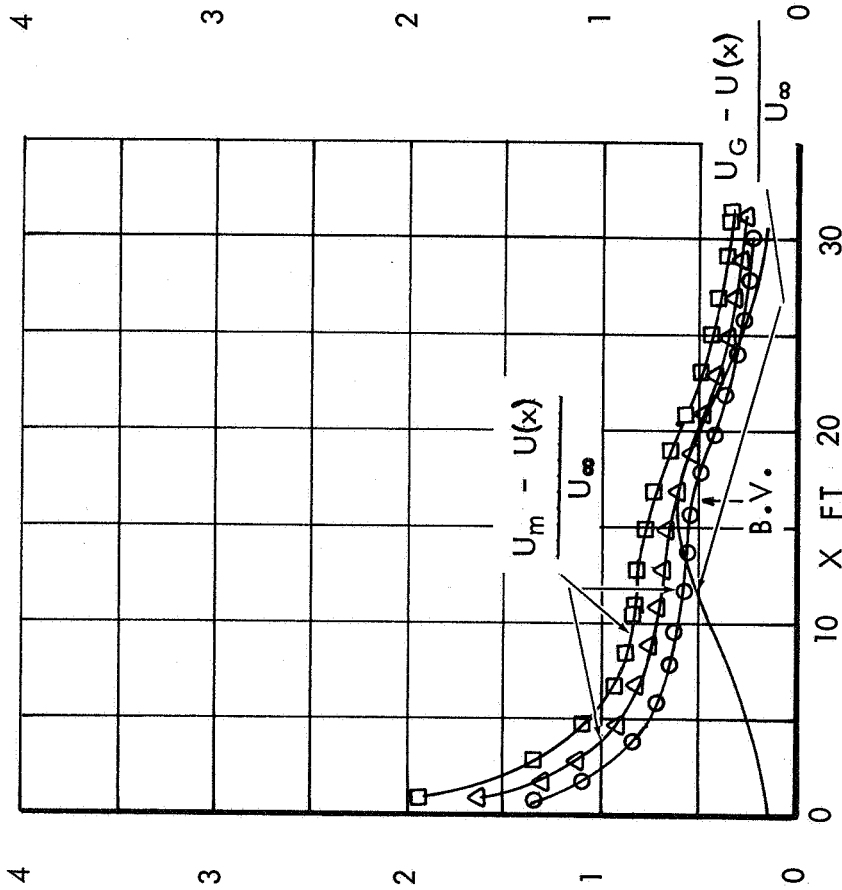
N = 2.5 △

N = 3 □

$$C_{1h}' = 4.00$$

$$C_{P_{MAX}} = 0.87$$

$$C_{P_{SLOT}} = 0.300$$



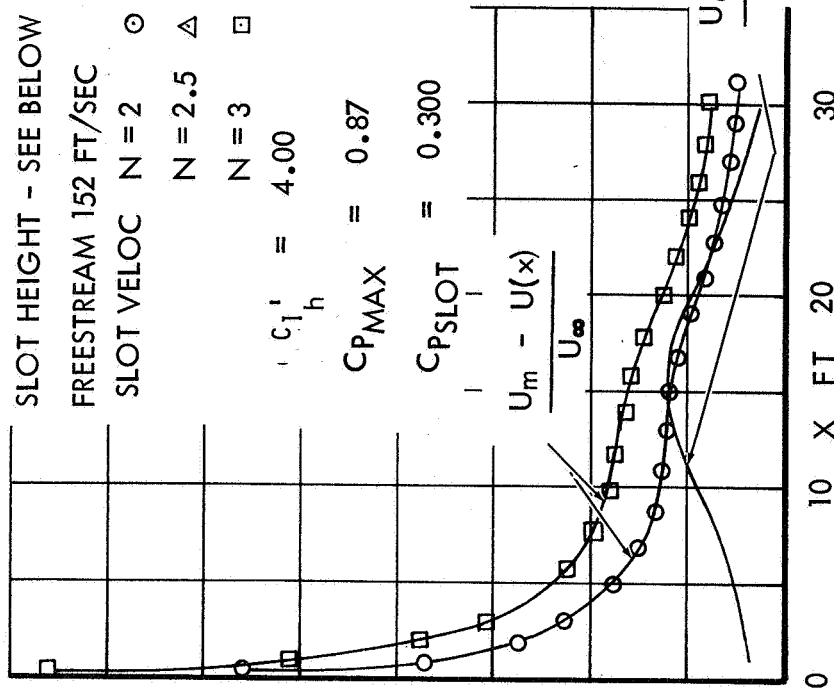
H_{SLOT} = 0.067 FT (0.805")

○ 345.0 FT/SEC (N = 2)

△ 390.0 FT/SEC (N = 2.5)

□ 442.0 FT/SEC (N = 3)

(a)



H_{SLOT} = 0.02665 FT (0.32")

○ 546.0 FT/SEC (N = 4.08)

□ 701.0 FT/SEC (N = 4.69)

} SAME THRUST AS (a)

(b)

FIGURE 24 EFFECT OF SLOT HEIGHT - HIGH REYNOLDS NUMBER

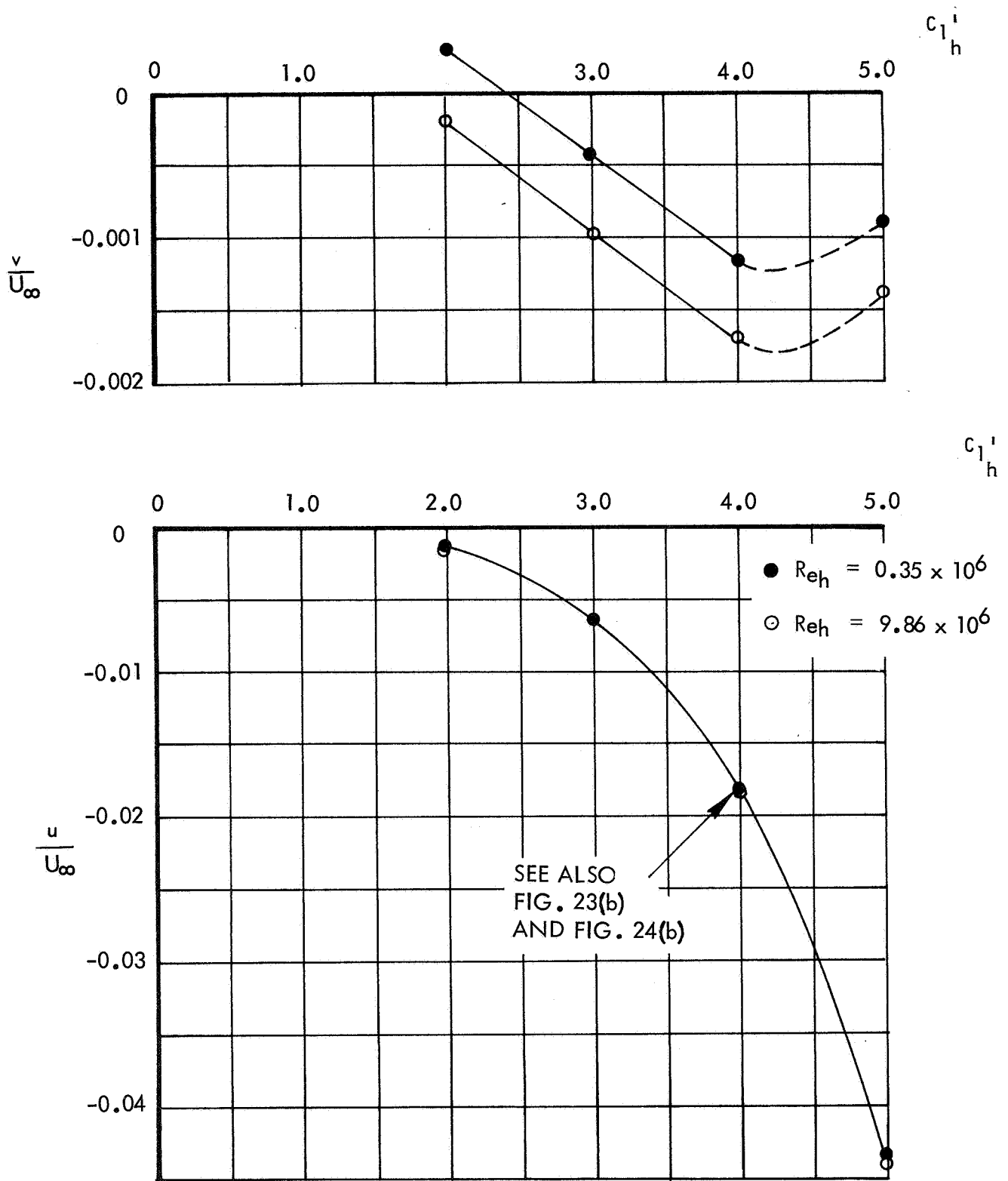


FIGURE 25 INDUCED FLOW, AT THE BOUND VORTEX, CAUSED BY ENTRAINMENT INTO A WALL-JET USED TO SIMULATE A MOVING GROUND.

NOTE: THE CORRESPONDING MOVING-GROUND AND FIXED-GROUND PLOTS ARE GIVEN IN FIGURES 12 AND 16, RESPECTIVELY.